Petroleum Science 23 (2026) 3739–3758

Contents lists available at ScienceDirect

Petroleum Science

journal homepage: www.keaipublishing.com/en/journals/petroleum-science

Original Paper

Formation and preservation processes of Ediacaran microbial dolomite pore system, evidence from the Qigebrak Formation, Tarim Basin, China

Xu-Dong Chen [a,b], Qi-Lu Xu [a,b,*], Fang Hao [a,d], Guo Yang [c], Ping Wang [c], Fei-Fei Yuan [a,b], Xin-Le Li [a,b], Jin-Qiang Tian [a,b], Guang-Wei Wang [a,b]

[a] State Key Laboratory of Deep Oil and Gas, China University of Petroleum (East China), Qingdao, 266580, Shandong, China
[b] School of Geosciences, China University of Petroleum, Qingdao, 266580, Shandong, China
[c] Research Institute of Exploration and Development, PetroChina Tarim Oilfield Company, Korla, 841000, Xinjiang, China
[d] Laboratory for Marine Mineral Resources, Qingdao National Laboratory for Marine Science and Technology, Qingdao, 266071, Shandong, China

A R T I C L E I N F O

Article history:
Received 27 December 2024
Received in revised form
19 August 2025
Accepted 31 October 2025
Available online 4 November 2025

Edited by Xi Zhang and Jie Hao

Keywords:
Tarim Basin
Ediacaran
Microbial dolomite
Pore system

A B S T R A C T

Ancient microbial dolomite reservoirs exhibit distinct advantages in both their formation and preservation processes, making them significant hosts for hydrocarbon resources. However, the interaction of multiple geological factors complicates the assessment of ancient microbial dolomite pore systems and the reconstruction of their differential evolutionary processes. This study investigates the morphological characteristics and evolution of pore systems within Ediacaran microbial dolomites. Through quantitative analysis of pore structures using nuclear magnetic resonance (NMR) T_2 curves, supplemented by petrographic and scanning electron microscopy observations, rock fabric analysis, a robust method for pore system identification based on four NMR T_2 curves was established. Comparative analysis of differential characteristics and evolutionary processes of pore systems in diverse microbial dolomite types. Spongiomicrobialite and stromatolite exhibit diverse primary porosity, including microbial mold and framework pores, as well as dissolution pores, resulting in a wide range of porosity. In contrast, residual microbial rocks are dominated by secondary pores, while thrombolite displays limited porosity. The effective preservation of microbial dolomite pores is influenced by the interaction between microbes and the Precambrian marine environment. Early microbially mediated dolomitization conferred significant resistance to compaction and pressure dissolution in microbial carbonates. In elevated terrains above the wave base or within the upper sections of highstand system tracts (HST) quasi-sequence groups, microbial dolomites rich in primary pores are more prone to dissolution by diagenetic fluids, which can modify original sedimentary structures. Conversely, environments characterized by poorly developed primary pores and restricted fluid flow tend to preserve the original structures.

1. Introduction

Microbial dolomite has advantages in pore systems formation and preservation (Luo et al., 2013; Song et al., 2014; Loucks, 2018). Precambrian examples show significant hydrocarbon potential, including microbial dolomite in the Oman Basin (Schröder et al., 2005; Mettraux et al., 2015; Smodej et al., 2019), the Wumishan Formation in North China (Yuan et al., 2022; Zhai et al., 2023), and the Dengying Formation in Sichuan Basin (Chen et al., 2017; Qu et al., 2020; Xu et al., 2022; Zhu et al., 2022; Song et al., 2024).

Conventional theory states reservoir porosity decreases by 1%–2%/Myr with age and 1%–3%/km with depth (Ehrenberg et al., 2012). However, dolomite reservoirs below 6000 m retain high porosity–permeability zones, defying the “porosity-death line” concept (Hao, 2022; Guo et al., 2023; Zhao et al., 2023b). Pore development arises from coupled processes: depositional–diagenetic feedbacks (Wang et al., 2023; Shen et al., 2024),

* Corresponding author.
E-mail addresses: xuqilu@upc.edu.cn, qilu_xu@outlook.com (Q.-L. Xu).
Peer review under the responsibility of China University of Petroleum (Beijing).

https://doi.org/10.1016/j.petsci.2025.10.032
1995-8226/

tectonic-stress interactions (Ma et al., 2024), and organic–inorganic interplay (Hao et al., 2015; Yuan et al., 2025). Microbial dolomites exhibit complex mechanisms where pore systems are governed by rock fabrics, microbial metabolism, and microbe-seawater interactions beyond conventional diagenesis (Grotzinger and Al-Rawahi, 2014; Zhu et al., 2020a; Hu et al., 2023).

Unique microbial textures form the basis for early primary pores. For instance, Upper Jurassic microbial carbonates in Brazil show stromatolites with connected pores, while thrombolites have complex pore systems from micrite clot variations (Rezende et al., 2013). These pore-throat networks are controlled by depositional textures. Microbial processes mediate coupled organic-inorganic reactions that drive carbonate precipitation and early dolomitization, enhancing chemical durability and mechanical compaction resistance (Schmoker and Halley, 1982; Ehrenberg et al., 2006). Pore systems are controlled by: (i) microbial metabolism (Shen et al., 2022), (ii) rock fabrics (Li et al., 2015b), (iii) depositional environments (Luo et al., 2013; Zhai et al., 2023), and (iv) diagenetic processes (Chen et al., 2017; Li et al., 2023). Documented examples include environmentally controlled Miocene carbonates in southeastern Spain (Lipinski et al., 2013) and burial-diagenesis modified Jurassic units in the Gulf of Mexico (Haddad et al., 2013).

A sequence of shallow marine tidal flat dolomite, approximately 200 m thick, was deposited in the Ediacaran Qigebrak Formation in the northwest Tarim Basin. It is the well-preserved primary rocks fabrics and pore structures of microbial dolomites, which constitute 90%–95% of the total volume, that make them an ideal laboratory for investigating ancient microbial dolomite pore systems. It experienced successive diagenetic processes: early dolomitization, dissolution, karstification, compaction, and cementation (Yan et al., 2019; Tang et al., 2022). Reservoir quality is controlled by multi-stage dissolution from sedimentary cycles and tectonic movements (Tang et al., 2022). Key destructive processes include shallow-burial cementation and deep compaction (Yang et al., 2020a), while preservation factors are early dolomitization and hydrocarbon emplacement (Chen et al., 2023).

The significance of microbial dolomite pore systems for reservoir prediction is widely recognized, yet their differential evolution mechanisms remain elusive. This study classifies and quantifies pore systems using four distinct NMR T_2 curves for identification. Comparative analysis of microbial dolomite types reveals differential pore characteristics and evolutionary processes. We establish controls of microbial activity, depositional environments, and diagenesis on multi-scale pore structures, and construct genetic connections between these factors and pore evolution. Consequently, this work provides an innovative approach to assess heterogeneity in deep ancient microbial dolomite reservoirs.

2. Geological setting

The Tarim Basin, situated in Xinjiang Province, northwestern China, is bounded by the Tianshan Mountains to the north and the Kunlun Mountains and the Altun Mountains to the south (Fig. 1(a)). Covering approximately 560,000 square kilometers, it holds paramount significance in China due to its abundant oil and gas reserves (Wang et al., 2024). In the Early Cryogenian, the Tarim Basin underwent continental margin rifting due to the fragmentation of the Rodinia supercontinent (Guan et al., 2017; Yang et al., 2021). Subsequently, as the tension diminished, it transitioned into a stage of rifting to depression during the Late Cryogenian–Early Ediacaran (Shi et al., 2018). In the Late Ediacaran period, the northwestern section of the basin experienced stabilized tectonic subsidence. Currently, the basin is in the depression evolution stage within the Craton Basin, characterized by the development of a depositional system of carbonate platform (Zhang et al., 2024).

In the Tarim Basin, during the Upper Ediacaran period, the Qigebrak Formation stands out as the predominant host of Precambrian microbial dolomite (Li et al., 2015a; Zhu et al., 2020a). The Qigebrak Formation constituted a gently sloping carbonate platform with sedimentary microfacies characterized by tidal flats, lagoons, and granular beach deposits (Wei et al., 2021; Yang et al., 2021). A mixed carbonate–siliciclastic tidal-flat environment predominated during the early stage of deposition of the Qigebrak Formation, while the late stage featured a carbonate platform, and the Tabei massif was the provenance of terrigenous detrital input in early mixed tidal flats (Zhao et al., 2023a; Chen et al., 2024). The study area experienced a shallow depositional environment characterized by warm and arid conditions during the Late Ediacaran period, influenced by the geological structure, climate, and sea level. The sedimentary water exhibited weakly oxidizing conditions and high salinity. The evolution of paleo-redox conditions in terminal Ediacaran shallow waters involved a gradual oxidation process, from suboxic to oxic environments.

The stratigraphic thickness of the Qigebrak Formation ranges from 110 to 240 m and is extensively exposed in the northwestern margin of the Tarim Basin (Fig. 1(b)). Its contact with both the underlying Sugetbulak Formation and the overlying Yurtus Formation is marked by a parallel unconformity (Fig. 1(c)). Based on lithofacies associations, sedimentary structures, and depositional environmental characteristics, the succession can be classified into four lithofacies association units designated as Q1, Q2, Q3, and Q4 (Zheng et al., 2021a, 2021b; Wang et al., 2022). Q1 mainly comprises the supratidal-intertidal zone, with oolitic dolomite, sandy debris dolomite, and minor sandstone and mudstone (Huang et al., 2025). Q2, deposited in a low-energy hydrostatic intertidal zone, mainly consists of thrombolites, flat laminated stromatolites, and spongiomicrobialites. Q3, in high-energy lower intertidal and supratidal zones, comprises thrombolites, wavy and domal stromatolites, and thick layers of spongiomicrobialites (Fig. 2). The microbial dolomite in this section, characterized by abundant and diverse pore systems, suggests its potential as an oil and gas reservoir (Yan et al., 2019; Chen et al., 2023). Q4, dominated by karst breccia dolomite, represents a high-quality reservoir in unconformity contact with the overlying Yuertusi Formation (Wu et al., 2021).

3. Samples and analytical methods

The results presented in this study are based on 2 deep-drilling cores of the Upper Ediacaran Qigebrak Formation in the northwest of the Tarim Basin (Fig. 1(a)) and 3 outcrops (Figs. 1(b) and 2). A total of 803 samples, including 255 thin sections and 224 core plugs, were analyzed. These samples were collected from the following locations: the Linkuanggou outcrop (161 samples, 19 thin sections), the Jianbizhenmutage outcrop (173 samples, 45 thin sections), the Aoyipikexigou outcrop (381 samples, 142 thin sections), the QT1 well (45 samples, 18 thin sections; depth: 5995–6005 m), and the LT1 well (43 samples, 31 thin sections; depth: 8600–8876 m).

Cast thin sections were cut from one end of permeability plugs, and therefore correspond with measured values of porosity, permeability and nuclear magnetic resonance (NMR), which permit direct comparison of the petrography with the petrophysical properties measured from the rocks. The 185 sections of these were impregnated with blue epoxy to determine the pore types. Under the standard polarizing light, the pore system shows bright blue. The cast thin sections were analyzed using the Leica

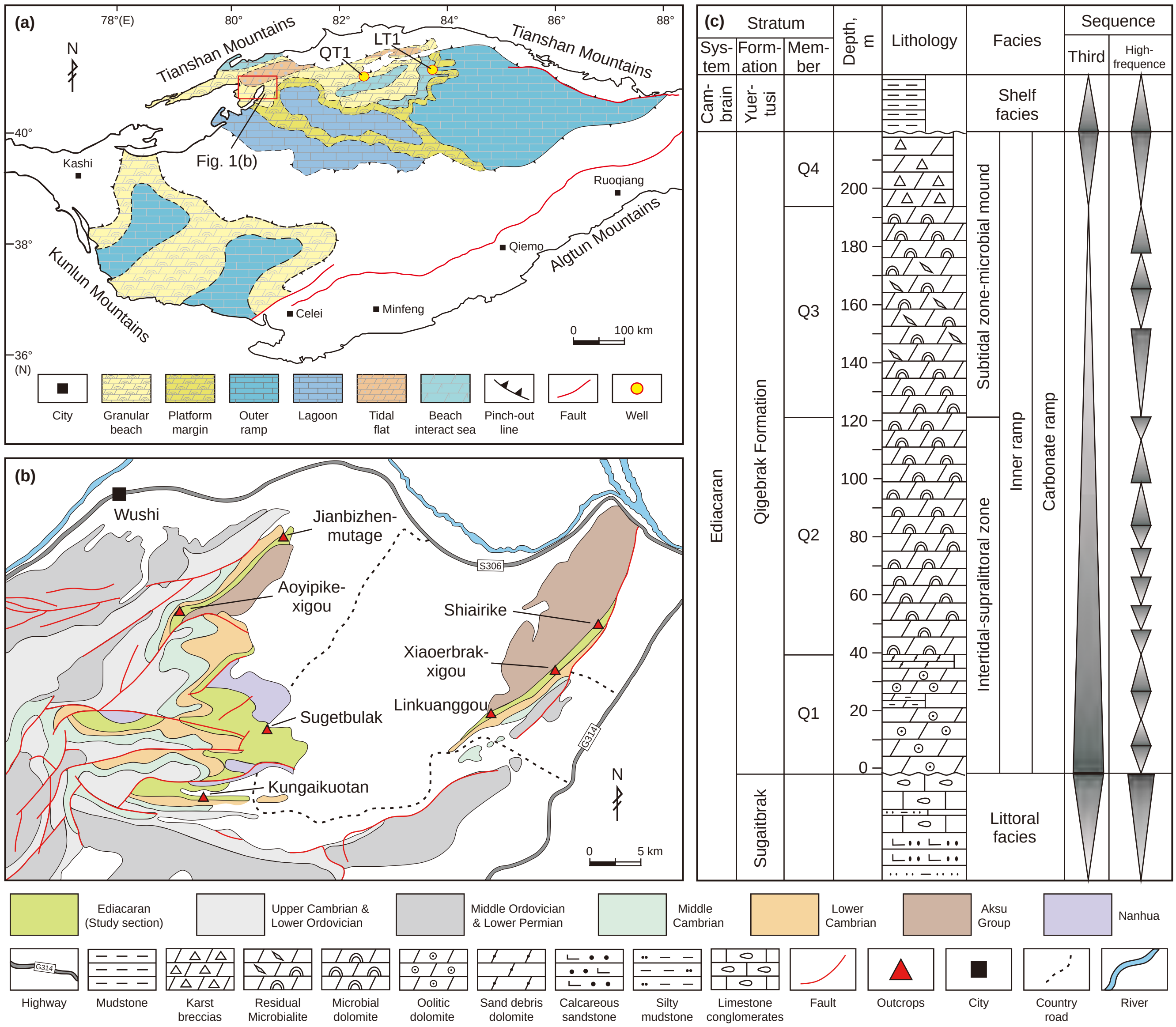

Fig. 1. (**a**) Geological situation in the study area, modified from Yang et al. (2021). (**b**) Distribution of the Ediacaran strata and field section locations in the northwest of the Tarim Basin. Note the localities of the studied sections, modified from Li et al. (2015b) and Wang et al. (2022). (**c**) Simplified lithological column of the Qigebrak Formation in the Aoyipikexigou outcrop.

DM6M automatic microscopic analysis system, enabling full-field image acquisition at the National Key Laboratory of Deep Oil and Gas, China University of Petroleum (East China). To obtain the area percentages of rock components like matrix, cement, and porosity, the casting thin section images were processed with Adobe Photoshop Quantification (PSQ) method, described by Zhang et al. (2014); Xu et al. (2022).

NMR analysis was conducted on cylindrical samples (2.5 cm in diameter) using the Mi-croMR23-060H-1, a medium-sized low-field NMR analyzer. The experimental method followed the SY/T6490-2007 Specification, widely used in the oil and gas industry for laboratory measurement of rock sample NMR parameters. To enable comparison of NMR T_2 spectra across varying sample sizes, the pore signal in these spectra was normalized by dividing signal intensity by sample volume. The quantity of various peaks in the T_2 spectra provides insight into the number of pore types, while the area of the peak reflects the size of the pores. Additionally, the area between peaks indicates the connectivity of pores or fractures (Xu et al., 2019; Liu et al., 2020). This paper employs the relationship established by Zhao et al. (2022) between the relaxation time T_2 and pore size to semiquantitatively describe the pore structure of the samples. In this framework, T_2 values less than or equal to 4 ms signify micropores, 4 ms < $T_2 \leq$ 100 ms denote mesopores, and T_2 values exceeding 100 ms indicate macropores.

Porosity was measured using an Ultrapore-300 Helium Porosimeter and horizontal permeability was measured on an WPH-300 Gas Permeameter. Besides, porosity measured by the helium gas expansion method is the ratio of pore volume and sample volume, unless otherwise specified, it is directly expressed as ‘porosity’. In contrast, Adobe Photoshop quantification results will be preceded by PSQ abbreviations.

To examine microbial dolomite's microporosity and mineral morphology, six samples were analyzed using SEM with a Crossbeam 550 dual-beam system. The analysis was conducted at the National Key Laboratory of Deep Oil and Gas, China University of Petroleum (East China) with an accelerating voltage of 10–20 kV.

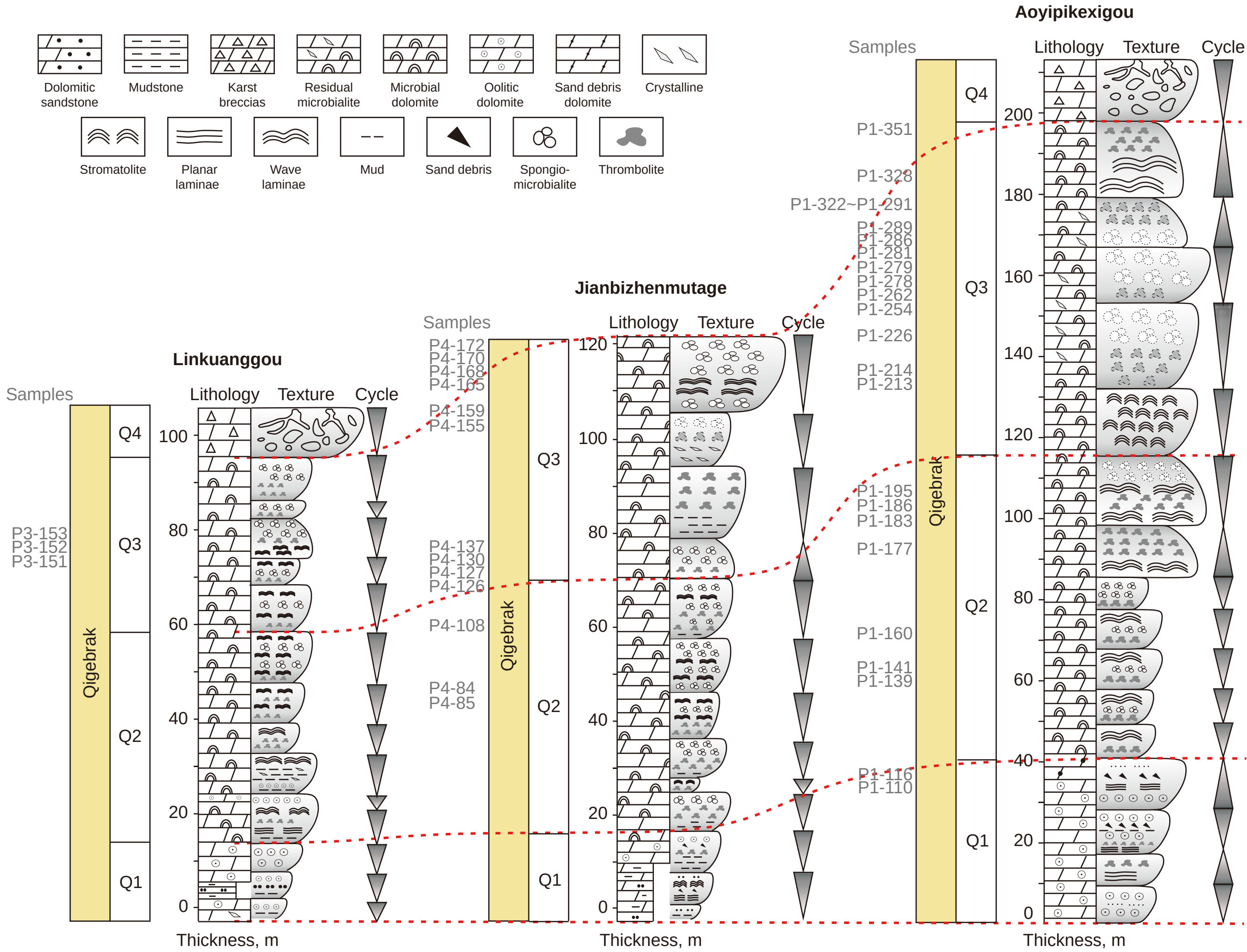

Fig. 2. Lithological column of the Qigebrak Formation in the Northwest of Tarim Basin.

4. Results

4.1. Lithofacies and multiscale pore system morphology

Stromatolite can be broadly categorized into three distinct types based on their morphological properties, namely domal, wavy and flat laminate (Hu et al., 2021). Domal stromatolite (Fig. 3(a)), characterised by their dome-shaped structures, are formed by the specific orientation of dolomite cylinders, with purplish-red clay infillings and carbonatite cement interspersed between them. The rounded shape of protrusions or depressions is observable on the top surface of these stromatolites (Fig. 3(b)). These stromatolites deposit in the peritidal to shallow-subtidal environment characterized by high-energy hydrodynamic conditions (Siahi et al., 2016; Xu et al., 2022). Domal stromatolite mainly develops in the third members of the Qigebrak Formation (Fig. (2)). Both the wavy stromatolite and the flat laminite stromatolite consist of dark and light laminations. The dark laminations often function as pore framework, and in certain areas, the light laminations are also visible as microbial pores, typically occupied by crystalline dolomite. The microbial-framework pores primarily develop within the light laminations of stromatolite, exhibiting a laminar distribution (Fig. 4(a)–(b)). Flat laminite stromatolite (Fig. 3(c)), with a more typical structure of bright and dark laminations, is developed mainly in low-energy subtidal zones of deeper water (Mettraux et al., 2015; Zheng et al., 2021a, 2021b). Wavy stromatolite, which is distinguishable by its mound-like protrusions when examined under a microscope (Fig. 3(g)–(h)), forms in a high-energy hydrodynamic environment (Zhai et al., 2023).

Thrombolite, a type of microbialite lacking stratified structure, is mainly formed by the benthic microbial community solidifying clastic sediments through capture and bonding or using its growth framework as a precipitation center (Mei, 2007). Macroscopically, thrombolites lack laminations, with only sparse discontinuous laminae or scattered mottled fabrics. Microscopically, foam-textured microbial laminations are rare, algal-rich components appear as filamentous or irregular clots, and filamentous microbial binding materials show disordered, continuous or discontinuous distributions without clear patterns. The thrombolites (Fig. 3(d)) are primarily composed of non-laminated, irregular dark clots, which are distributed either discretely or continuously. Microbial framework pores between clots are typically filled by multigenerational dolomite cementation, with cement crystals ranging from 50 to 200 μm in size (Fig. 3(e)–(f)). The interior of the clots is micritic, mainly composed of micritic dolomite particles measuring 5–50 μm in diameter. Similar to planar stromatolites, these clotted microbialites predominantly formed in deep-water, low-energy subtidal environments (Suarez et al., 2019).

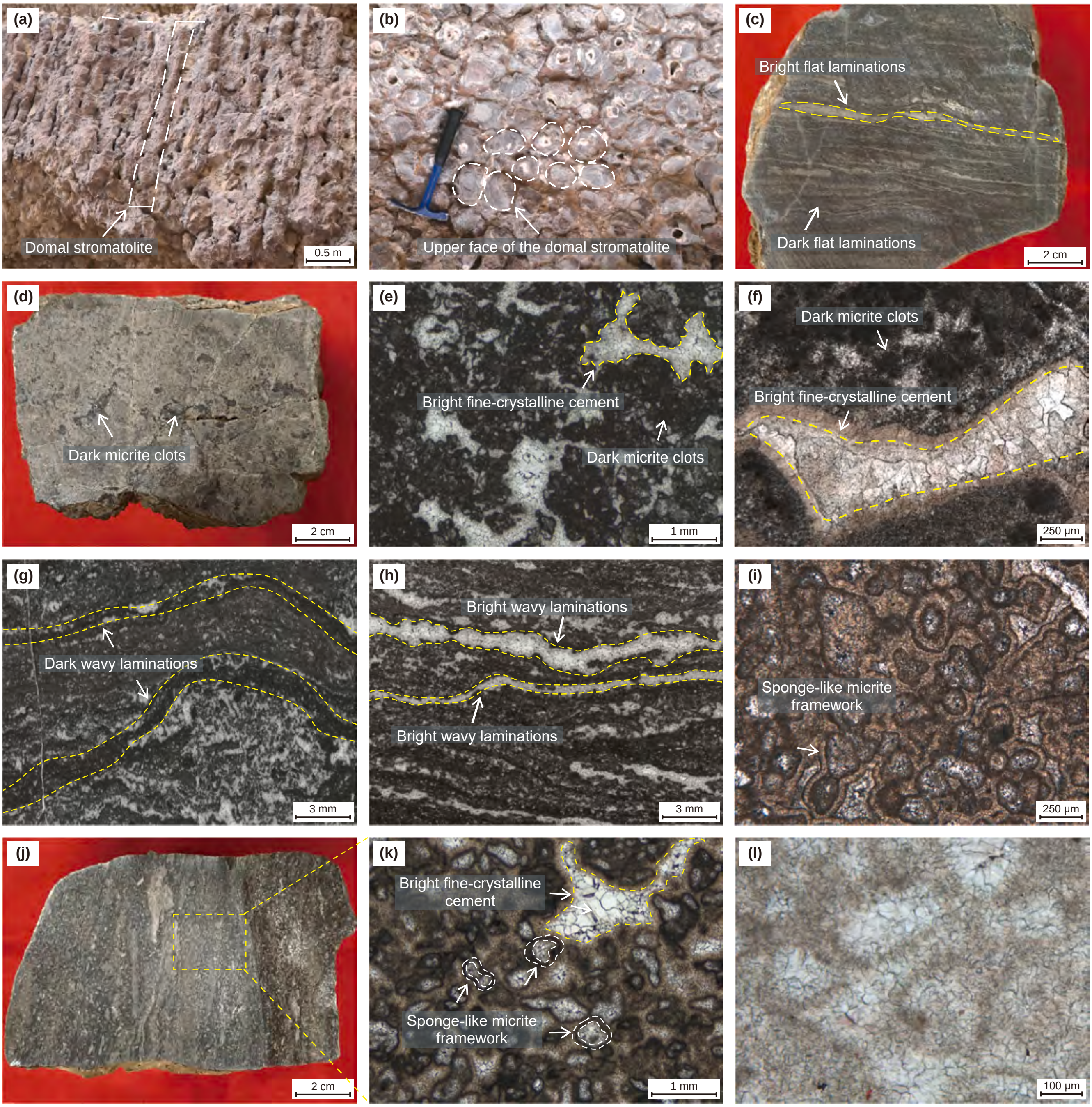

Fig. 3. Lithofacies types of Qigebrak Formation, the samples were collected from the Aoyipikexigou outcrop ((a), (b), (c), (d), (e), (g), (h), (j), (k)) and ultra-deep wells in the Tarim Basin. (**a**) Domal stromatolite; (**b**) the top of domal stromatolite; (**c**) flat laminated stromatolite; (**d**), (**e**) thrombolite; (**f**) thrombolite, Well LT1, 8703 m; (**g**), (**h**) wave stromatolite; (**i**) spongiomicrobialite, Well QT1, 6002.4 m; (**j**), (**k**) spongiomicrobialite; (**l**) residual microbialite, Well LT1, 8710 m.

Spongiomicrobialite is a type of microbial dolomite that lacks laminated structures but exhibits a sponge-like framework on meso-scale (Li et al., 2015b). Under the microscope, the spongy texture, which is composed of the rounded or subrounded micrite cladding and the inner cavity (Fig. 3(i)–(k)). The size of a single micrite cladding varies from 10 to 1000 μm. These claddings are closely packed and sometimes in floating contact. Consequently, the resulting lattice framework presents a foamy, honeycomb, or spongy structure. The microbial-framework pores in spongiomicrobialite range from 50 to 200 μm in size, wherein the micrite cladding constitutes the framework (Fig. 4(a)–(b)). The microbial-mold pores within the inner cavities typically display a rounded or subrounded shape, with pore diameters varying from 100 to 500 μm (Fig. 4(c)–(d)). During the diagenetic process, these pores were either fully or partly infilled with dolomite cement, as shown in (Fig. 4(e)). Spongiomicrobialite is primarily developed in the intertidal to subtidal zone characterized by strong hydrodynamic conditions. Within the study area, it is particularly developed in the third members of the Qigebrak Formation (Fig. (2)).

The microbial dolomite in the Qigebrak Formation has undergone diagenetic processes, including dolomitization, dissolution, and recrystallization, as reported by Tang et al. (2022) and Chen

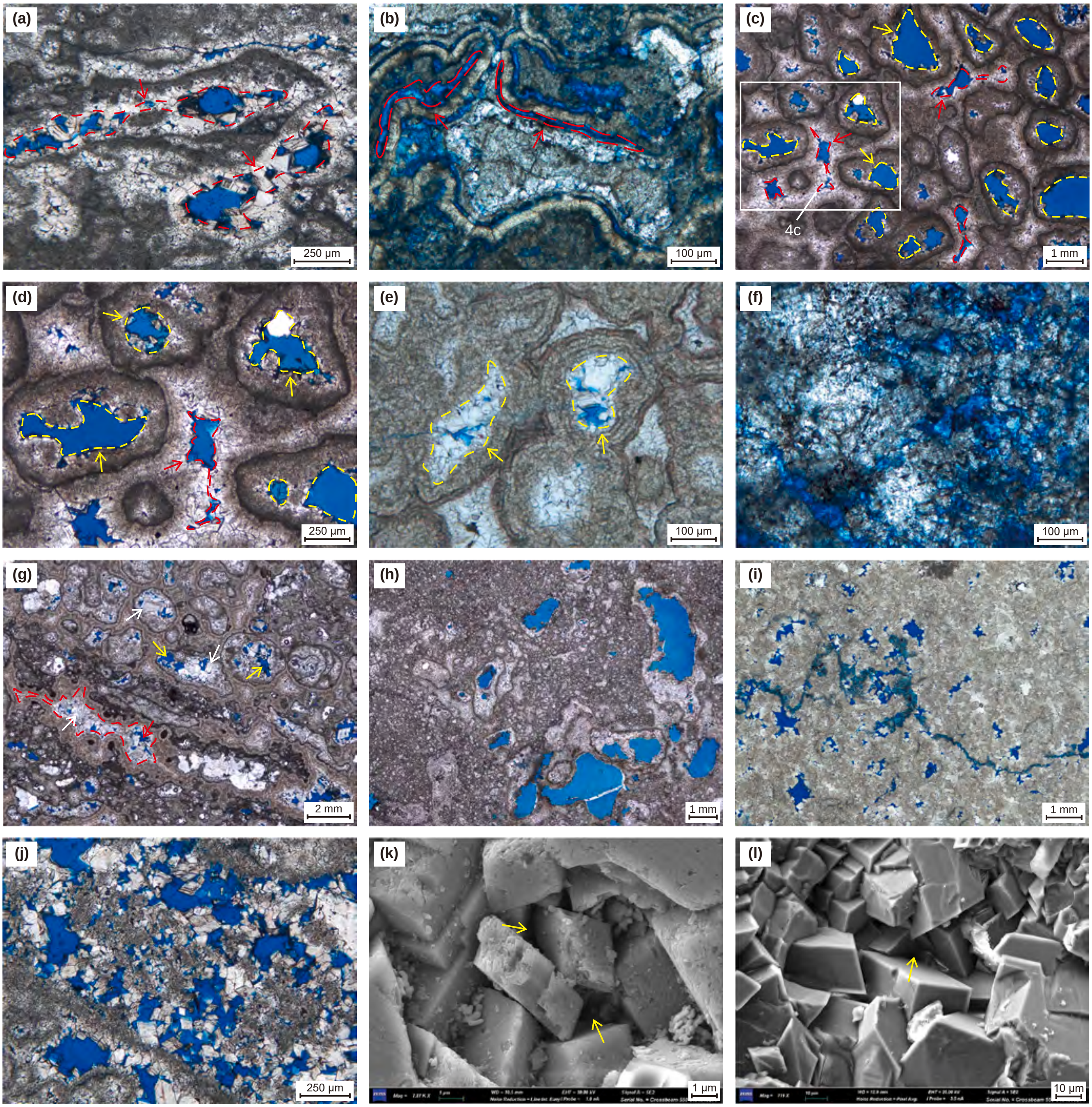

Fig. 4. Photomicrographs showing different types of pores in microbial dolomite of the Qigebrak Formation. (**a**) Microbial-framework pores in stromatolite, red arrows, Linkuanggou outcrop, blue cast thin section; (**b**) microbial-framework pores, red arrows, Well QT1, 6004.3 m; (**c**), (**d**) microbial-framework pores and microbial-mold pores in spongiomicrobialite, red arrows point to microbial-framework pores, yellow arrows point to microbial-mold pores, Jianbizhenmutage outcrop; (**e**) microbial-mold pores, yellow arrows, Well QT1, 6005 m; (**f**) dissolution pores and fractures in residual microbialite, Well QT1, 6002.7 m; (**g**) microbial-mold pores, microbial-framework pores and dolomite cement in spongiomicrobialite, red arrows point to microbial-framework pores, yellow arrows point to microbial-mold pores, white arrows point to dolomite cement, Jianbizhenmutage outcrop; (**h**) dissolution caves in spongiomicrobialite, Jianbizhenmutage outcrop; (**i**) dissolution pores and fractures, Aoyipikexigou outcrop; (**j**) dissolution pores and intercrystalline pores, Jianbizhenmutage outcrop; (**k**), (**l**) SEM image displaying the intercrystalline pores between dolomite crystals, yellow arrows, Aoyipikexigou section.

et al. (2023). These processes have resulted in the formation of non-fabric dissolution pores (Fig. 4(f) and (h)) and fractures (Fig. 4(g)). Due to tectonic activity or diagenetic fluid transformation, the original fabric of the rock has been modified, leading to the growth of coarser dolomite crystals and the formation of fractures (Fig. 4(i)–(j)) and intercrystalline pores (Fig. 4(k)–(l)). The residual structural microbial dolomite has lost its primary sedimentary structure and only retains a small amount of dark microbial laminae and microbial frameworks under the microscope (Fig. 3(l)).

4.2. Different fabric content distribution in microbial dolomite

The quantitative microscopic analysis of the composition of 67 microbial dolomites is presented in Table 1 and depicted in Fig. 5. The characteristics of the matrix, cement, predominant pore types,

Table 1
Summary of Adobe Photoshop quantification (PSQ) data of microbial dolomite fabric.

Lithology type	Matrix context, %		Fabric selective pore context, %			Non-fabric selective pores context, %		Cement context, %
	Micrite clot/Crystal grain	Microbial framework	Microbial-framework pores	Microbial-mold pores	Intercry-stalline pores	Dissolution pores and caves	Fracture	Cement
Spongiomicrobialite	0.00 to 90.84 (46.08 ± 27.71)	2.36 to 79.93 (32.09 ± 24.75)	0.00 to 5.10 (1.53 ± 1.79)	0.00 to 20.65 (5.91 ± 6.11)	0.00 to 4.21 (1.00 ± 1.49)	0.00 to 20.18 (2.26 ± 4.62)	0.00 to 3.59 (0.45 ± 0.88)	0.00 to 29.21 (10.67 ± 10.35)
Stromatolite	0.00 to 57.5 (28.56 ± 18.81)	12.89 to 67.01 (44.73 ± 19.19)	0.82 to 9.56 (4.06 ± 2.81)	0.00 to 3.49 (0.96 ± 1.13)	0.00 to 2.03 (0.31 ± 0.66)	0.00 to 3.89 (1.03 ± 1.44)	0.00 to 6.11 (0.69 ± 1.81)	6.62 to 33.47 (19.66 ± 7.66)
Thrombolite	12.81 to 89.61 (53.48 ± 26.52)	0.00 to 60.08 (28.72 ± 19.49)	0.00 to 2.25 (0.61 ± 0.81)	0.00 to 1.18 (0.57 ± 0.41)	0.00 to 0.94 (0.19 ± 0.35)	0.00 to 1.21 (0.18 ± 0.42)	0.00 to 3.65 (0.92 ± 1.3)	0.00 to 41.11 (15.32 ± 11.09)
Residual microbialite	19.44 to 97.54 (80.59 ± 16.63)	0.00 to 63.03 (9.39 ± 13.44)	0.00 to 2.45 (0.15 ± 0.54)	0.00 to 1.11 (0.12 ± 0.27)	0.00 to 9.65 (2.57 ± 2.36)	0.00 to 10.03 (3.01 ± 2.52)	0.00 to 1.97 (0.35 ± 0.57)	0.00 to 25.33 (3.82 ± 5.92)

*Mean value ± standard deviation.

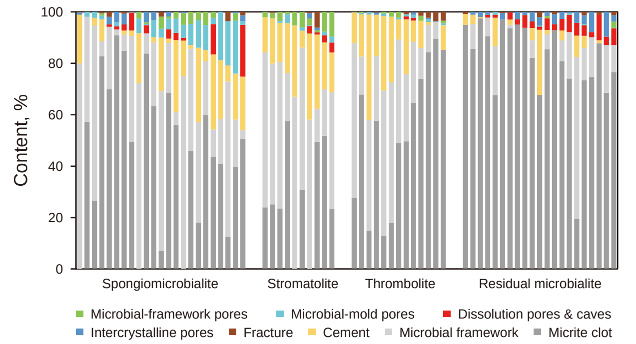

Fig. 5. Histograms showing PSQ-content distribution of the matrix (micrite clot and microbial framework), pores (microbial-framework, mold pores, dissolved pores & caves and intercrystalline pores), cement and fracture.

and PSQ content across different types of microbial dolomites are illustrated in Fig. 6.

The matrix of microbial dolomite consists of microbial framework and micrite clot. In spongiomicrobialite, the microbial framework content ranges from 2.36% to 79.93% with an average of 32.09%, while in stromatolite, it ranges from 12.89% to 67.01% with an average of 44.73%. Thrombolite exhibits a lower microbial lattice shelf content, ranging from 0 to 60.08% with an average of 28.72%, compared to the first two microbialites. The micrite clot content in thrombolite ranges from 12.81% to 89.61% with an average of 53.48%. In spongiomicrobialite, the micrite clot content varies widely from 0 to 90.84% with an average of 46.08%, while in stromatolite, it ranges from 0 to 57.5% with an average of 28.56%. Additionally, residual microbialite exhibits a dolomite grains content ranging from 19.44% to 97.54% with an average of 80.59%, and a relatively low average microbial framework content of 9.39% due to diagenetic influences. The highest cement content is observed in stromatolite, with an average value of 19.66%, while thrombolite and spongiomicrobialite have the second highest cement content, averaging 15.32% and 10.67%, respectively (Table 1, Fig. 5).

The primary pore types within the microbial dolomite of the Qigebrak Formation are microbial-framework pores (Fig. 4(a)–(d)) and microbial-mold pore (Fig. 4(b)–(e)), associated with microbial depositional tectonics. Dissolution pores and caves (Fig. 4(f)), intercrystalline pores (Fig. 4(g)–(i)), and fractures (Fig. 4(i)), linked to diagenesis, are also significant reservoir components. Stromatolite exhibits an average of 4.06% microbial-framework pores, while spongiomicrobialite and thrombolite show averages of 1.53% and 0.61%, respectively. Spongiomicrobialite is distinguished by a notable prevalence of microbial-mold pores, with an average of 5.91%, in comparison to 0.96% in stromatolite and 0.57% in thrombolite. Intercrystalline pores average 2.57% in residual microbialite, whereas in other types of microbial dolomite, it is less than 1%. Dissolution pores and caves are primarily found in residual microbialite, with an average content of 3.01% due to diagenesis. The variation in the average content of fractures among different types of microbial dolomite is less than 0.5% (Table 1, Fig. 5).

4.3. Nuclear magnetic resonance (NMR) results

NMR has been widely used to identify the complex pore structures of super-deep dolomite reservoirs in the Tarim Basin (Lai et al., 2020). The NMR results for 53 microbial dolomite samples are depicted in Fig. 7, illustrating four distinct NMR T_2 curves spectral features: multi-peak and high signal T_2 curves (MHT), double-peak T_2 curves (DPT), single-peak T_2 curves (SPT), and multi-peak and low signal T_2 curves (MLT).

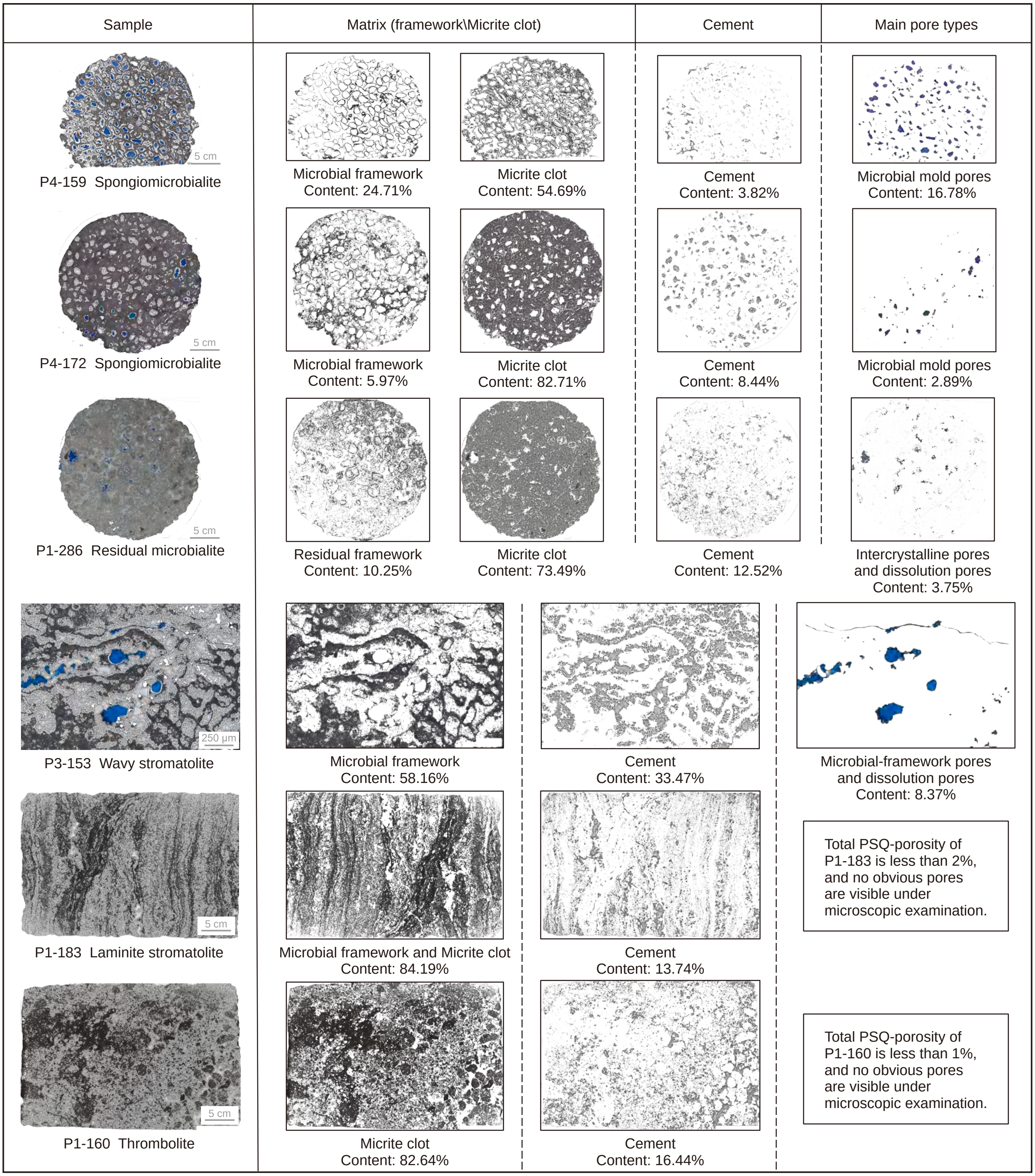

Fig. 6. Decomposition characteristics and PSQ content variability in microbial dolomites.

The MHT is characterized by multi-peak T_2 curves and high pore signal. These peaks distributed across three ranges: 0–4 ms, 4–100 ms, and >100 ms (Fig. 7(a)–(c)). The curves indicate the presence of intricate, multi-scale pore types, which are typically associated with higher porosity.

The DPT has the double-peak T_2 distribution and high & medium pore signal. The T_2 curves exhibit a clear bimodal distribution. The initial peak, observed between 10 and 100 ms, corresponds to medium-sized pores, while the second peak, between 200 ms and 2000 ms, is indicative of large pores (Fig. 7(d)–(e)).

The SPT has a single-peak T_2 distribution and medium pore signal. The T_2 distribution is mainly concentrated in 10–100 ms. The peak distribution of SPT in spongiomicrobialite ranges from 100 to 1000 ms (Fig. 7(g)–(i)), whereas in residual microbialite and thrombolite, it ranges from 4 to 100 ms.

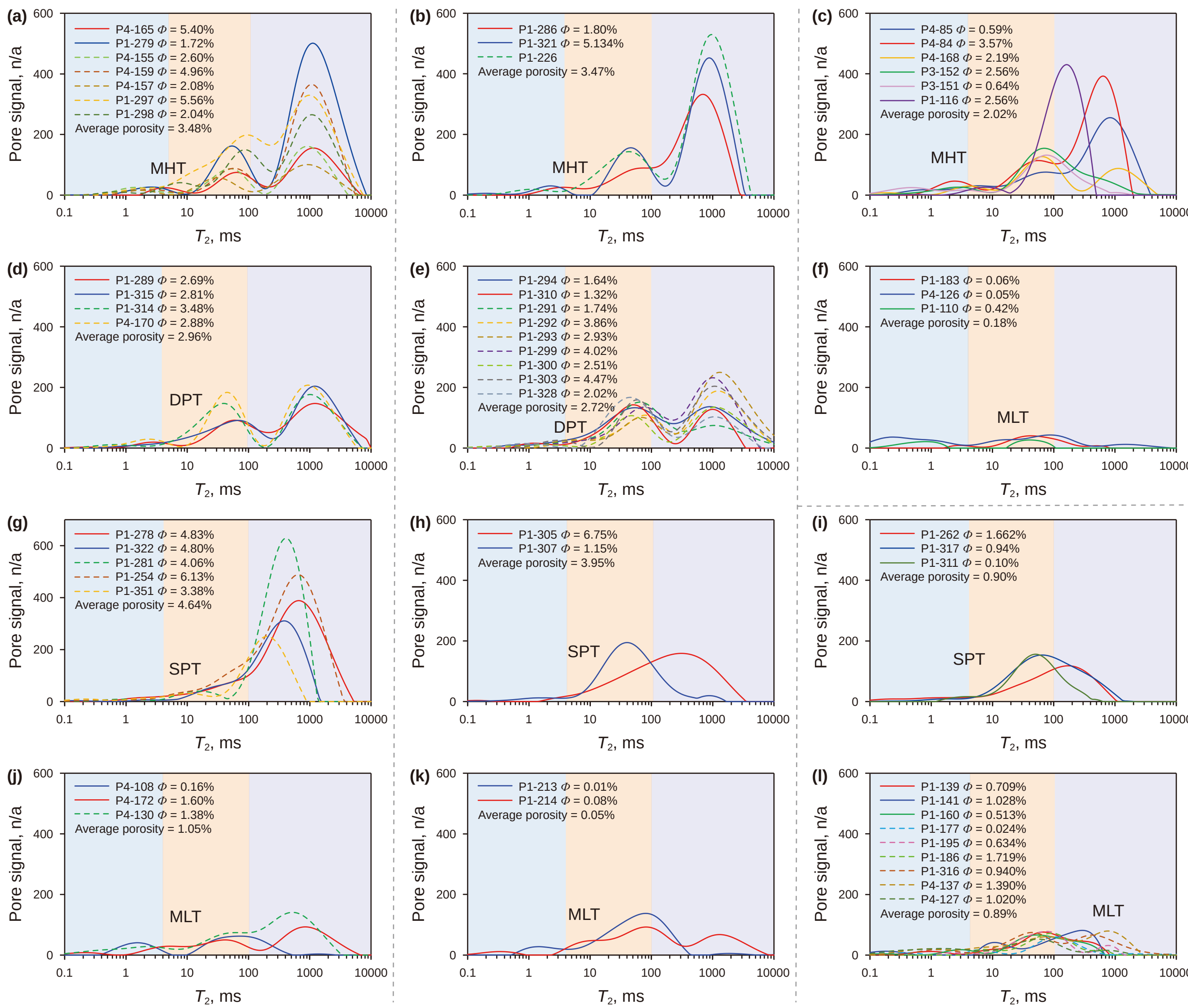

Fig. 7. NMR T_2 curves characteristics of microbial dolomite in the Qigebrak Formation. (**a**) Multi-peak and high signal T_2 curves (MHT) in spongiomicrobialite. (**b**) MHT curves in residual microbialite. (**c**) MHT curves in stromatolite. (**d**) Double-peak T_2 curves (DPT) in spongiomicrobialite. (**e**) DPT curves in residual microbialite. (**f**) Multi-peak and low signal T_2 curves (MLT) in stromatolite. (**g**) Single-peak T_2 curves (SPT) in spongiomicrobialite. (**h**) SPT curves in residual microbialite. (**i**) SPT curves in thrombolite. (**j**) MLT curves in spongiomicrobialite. (**k**) MLT curves in residual microbialite. (**l**) MLT curves in thrombolite.

The MLT has peakless and low pore signal T_2 curves, the porosity is generally lower than 2%. Consequently, the MLT are indicative of a high prevalence of micropores, which is consistent with the presence of a low-porosity pore system (Fig. 7(f) and (g)–(l)). Of note, the MLT are particularly prevalent in thrombolite samples.

4.4. Pore system differences in microbial dolomite

The results reveal a range of pore characteristics in microbial dolomite, from micrometer-scale intergranular pores to larger macroscopic pores, and from primary microbial-associated pores to secondary dissolution pores. These features show considerable variability among different types of microbial dolomites. The intricate pore structure results in a variation in microbial dolomite permeability by 2–3 orders of magnitude.

The porosity of the spongiomicrobialite varies widely, with a minimum porosity of 0.06%, a maximum of 14.84%, and an average of 3.79%. The stromatolite has good reservoir properties, with porosities ranging from 0.06% to 8.87%, with an average of 3.78% (Fig. 8). The spongy framework in spongiomicrobialite and the laminated framework in stromatolite are conducive to primary pore formation. This primary pore system, abundant in both types, facilitates diagenetic fluid transport, resulting in the enrichment of secondary dissolution pores and cement. The porosity of residual microbialite is between 0.01% and 7.96%, with an average of 3.52%. The porosity ranges from 2% to 5%. The residual microbialite of the Qigebrak Formation underwent significant diagenetic alteration, resulting in the modification of sedimentary texture and primary pores. The porosity of thrombolite is 0.007%–5.58%, with an average of 1.22%. The porosity distribution of most thrombolite samples ranges from 0% to 3%. Thrombolite exhibits a higher concentration of micrite clots characterized by significant variations in size, shape, and sortability. The predominant pore types in thrombolite are a limited number of primary pores and isolated solution pores (Fig. 9).

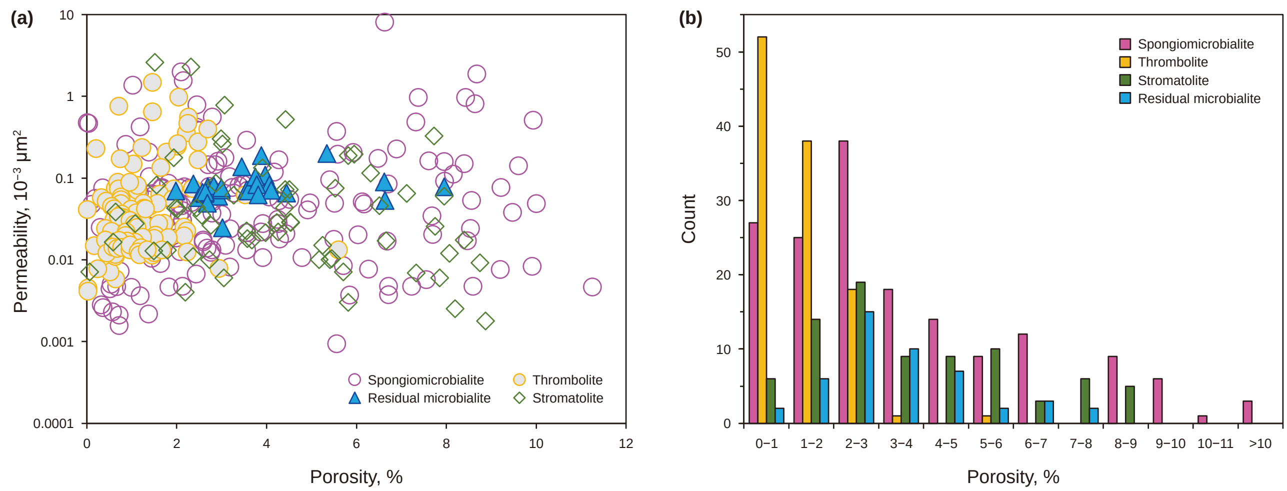

Fig. 8. (**a**) Cross-plots of porosity versus permeability value of the Qigebrak Formation microbial dolomite, a section of data sourced from Yan et al. (2019), Chen et al. (2020), Tang et al. (2022), and Chen et al. (2023). (**b**) Histogram of pore distribution in microbial dolomite of the Qigebrak Formation.

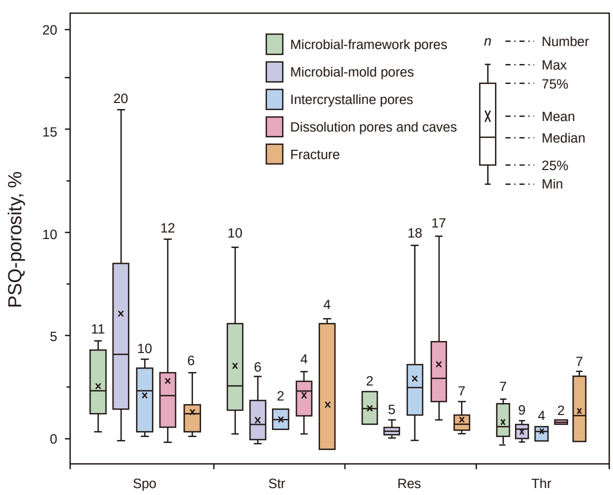

Fig. 9. Box plots showing PSQ-porosity distribution across various pore types in microbial dolomites. Spo: spongiomicrobialite; Str: stromatolite; Res: residual microbialite; Thr: thrombolite.

5. Discussion

5.1. Characterization of microbial dolomite pore systems in response to NMR

The pore type, morphology, size and PSQ-porosity of the microbial rocks of the MHT show a certain correlation (Fig. 10). Spongiomicrobialite and stromatolite of MHT predominantly feature microbial-associated pores, such as microbial-mold pore (Fig. 10(a)–(b)) and microbial-framework pores (Fig. 10(c)–(d)), with few dissolution pores and cavities. Conversely, residual microbialite of MHT exhibits a higher presence of intercrystalline pores and dissolution pores and cavities (Fig. 10(e)–(f)). The T_2 curves of the MHT in three distinct lithological samples exhibited peaks of pore signals across various relaxation time intervals, suggesting the existence of multiscale pores including micropores, mesopores, and macropores within the samples (Fig. 10(g)). The microscopic quantitative statistics are also consistent with the fact that almost all samples from the MHT are rich in pore types and also have high PSQ-porosity (5%–25%) (Fig. 10(h)).

The pore system exhibits various types of pores, differing in size and shape, facilitating favorable conditions for hydrocarbon storage and transport. Thus, the MHT T_2 curves likely signify a diverse and multiscale pore system within microbial dolomite.

The microbial dolomite of DPT shows significant diagenetic alteration, with the original morphology of the microbial-related pores altered. Microbial-framework and microbial-mold pores in spongiomicrobialite underwent varying degrees of dissolution and cementation (Fig. 11(a)–(c)), leaving only a few primary pores intact. The pore types found in residual microbialite mainly comprise intercrystalline pores, dissolution pores, and cavities (Fig. 11(d)–(f)), with their formation closely linked to mineral recrystallization and dissolution during diagenesis (Zhang et al., 2011). The T_2 curves of DPT microbial dolomite exhibit a distinctive “double-peak” pattern (Fig. 11(g)). The quantitative analysis of rock texture reveals that the DPT samples have a PSQ porosity of approximately 10%. Within this, intercrystalline pores, dissolution pores, and cavities exhibit PSQ porosities of around 5%. Pores associated with microbial activity and fractures demonstrate PSQ-porosity ranging from 1% to 2% (Fig. 11(h)). Hence, DPT T_2 curves typically indicate a pore system primarily characterized by intergranular and dissolution pores.

The SPT microbial dolomite typically exhibits a single predominant pore type, with only one to two pore types present in the majority of the tested samples. Sample P1-278 contained only a small number of microbial-framework pores and microbial-mold pore with uniform sizes (Fig. 12(a)–(b)). In Sample P1-307, intercrystalline pores predominated and exhibited uniform sizes (Fig. 12(c)–(d)). Sample P1-317 displayed a scarcity of microbial-mold pore (Fig. 12(e)–(f)). The pore diameters of P1-278 are notably larger than those of P1-307 and P1-317, leading to variations in their SPT T_2 curves. Specifically, the peak relaxation time of P1-278 ranges from 500 to 1000 ms, whereas the peak relaxation times of P1-307 and P1-317 range from 50 to 100 ms (Fig. 12(g)). In addition, P1-278 has a higher pore signal than the other two. The SPT typically indicates pore systems characterized by a single primary pore type, fewer secondary pores, and uniform pore size (Fig. 12(h)).

Most MLT microbial dolomite samples lacked obvious primary microbial-related pores, with rare instances of dissolution pores. Primary textures such as foamy microbial framework (Fig. 13(a)–(b)), microbial lamination structures (Fig. 13(c)–(d)), and micrite clot (Fig. 13(e)–(f)) were well preserved. MLT T_2 curves typically lack distinct characteristic peaks or exhibit low peak pore signals (Fig. 13(g)), with porosity usually below 2% (Fig. 13(h)).

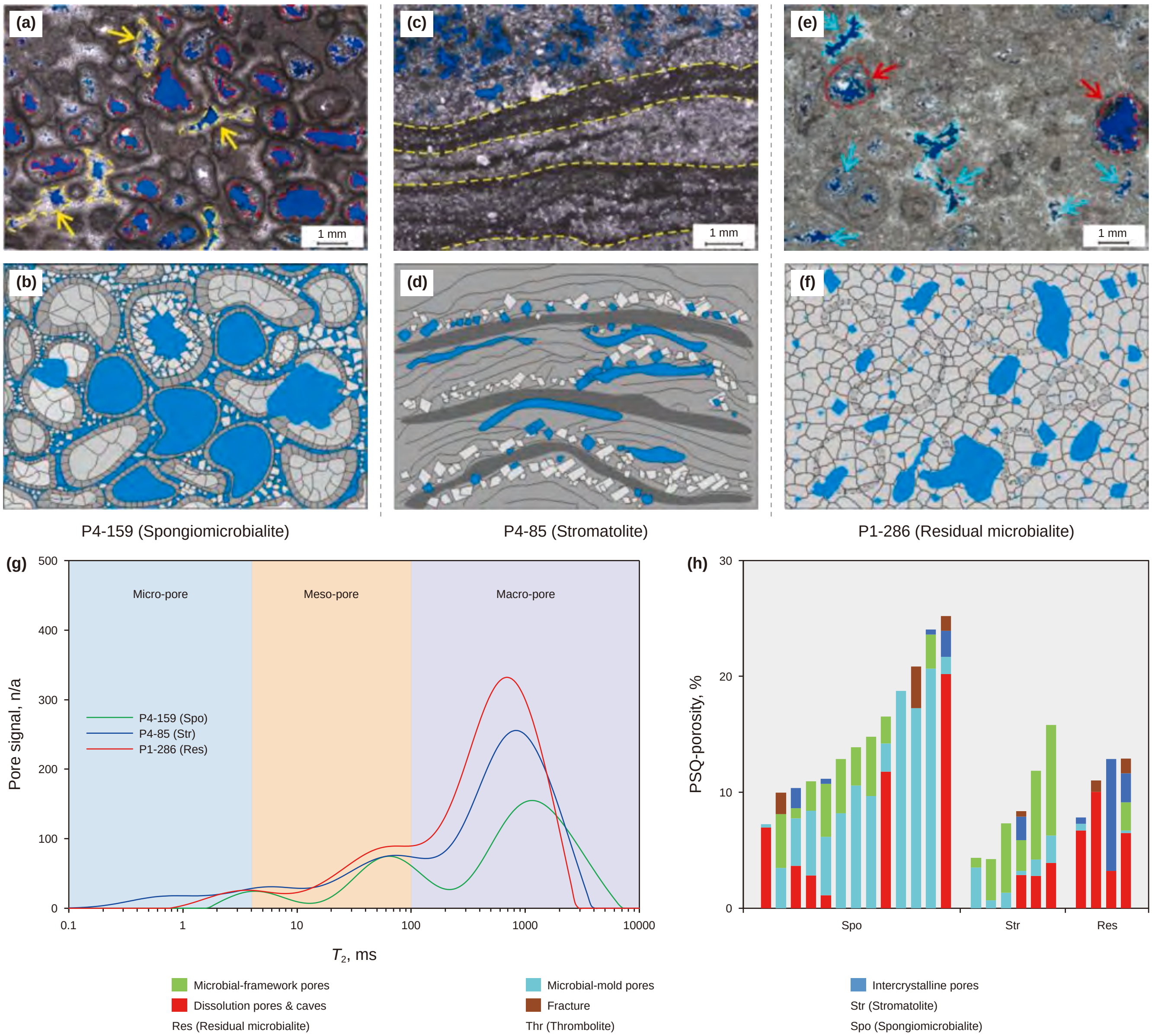

Fig. 10. Comparison of pore morphology, T_2 curves, and PSQ statistics for MHT microbial dolomite. (**a**) Pore morphology in spongiomicrobialite: casting sheet image of P4-159. (**b**) Simplified diagram of the MHT pore system in spongiomicrobialite. (**c**) Pore morphology in stromatolite: casting sheet image of P4-85. (**d**) Simplified diagram of the MHT pore system in stromatolite. (**e**) Pore morphology in residual microbialite: casting sheet image of P1-286. (**f**) Simplified diagram of the MHT pore system in residual microbialite. (**g**) T_2 curves of MHT microbial dolomite. (**h**) PSQ-porosity of MHT microbial dolomite.

Therefore, MLT generally signifies a pore system characterized by the absence of both primary microbial-associated pores and secondary dissolution pores.

In conclusion, the T_2 curves accurately portray the distinct pore structure characteristics of various types of microbial dolomites. This provides a solid foundation for comprehensive understanding and differentiation of these rock pore systems. NMR T_2 curves is dominant for a specific type of microbial dolomite. Specifically, MHT and SPT are prevalent in spongiomicrobialite (Figs. 10 and 12). DPT is dominant in residual microbialite (Fig. 11), and MLT is predominant in thrombolite (Fig. 13).

5.2. Vertical differentiation of pore systems controlled by high-frequency depositional cycles

High-frequency sedimentary cycles orchestrate vertical pore system differentiation through the coupling mechanism of microbial dolomite fabric construction and penecontemporaneous fabric-selective dissolution (Wang et al., 2023). In the vertically multi-cycle dolomite system of the Qigebrak Formation in Well QT1 (Fig. 14(a)), spongiomicrobialites developed in the middle-upper parts of shallowing-upward cycles. These dolomites contain microbial-framework pores and microbial-mold pores, which underwent penecontemporaneous meteoric freshwater fabric-selective dissolution, forming MHT/DPT-type T_2 curves. The vertical distribution of nuclear magnetic resonance (NMR) T_2 curves shows a strong correlation with porosity cyclicity (Fig. 14(b)–(c)). In contrast, thrombolites at the lower parts of cycles, constrained by low-energy depositional environments, are dominated by MLT-type T_2 curves (Fig. 13(g)).

This discrepancy originates from two key aspects: On the one hand, the vertical variations in dolomite fabric and textures controlled by high-frequency sedimentary cycles govern pore types and distribution. For instance, spongiomicrobialites are

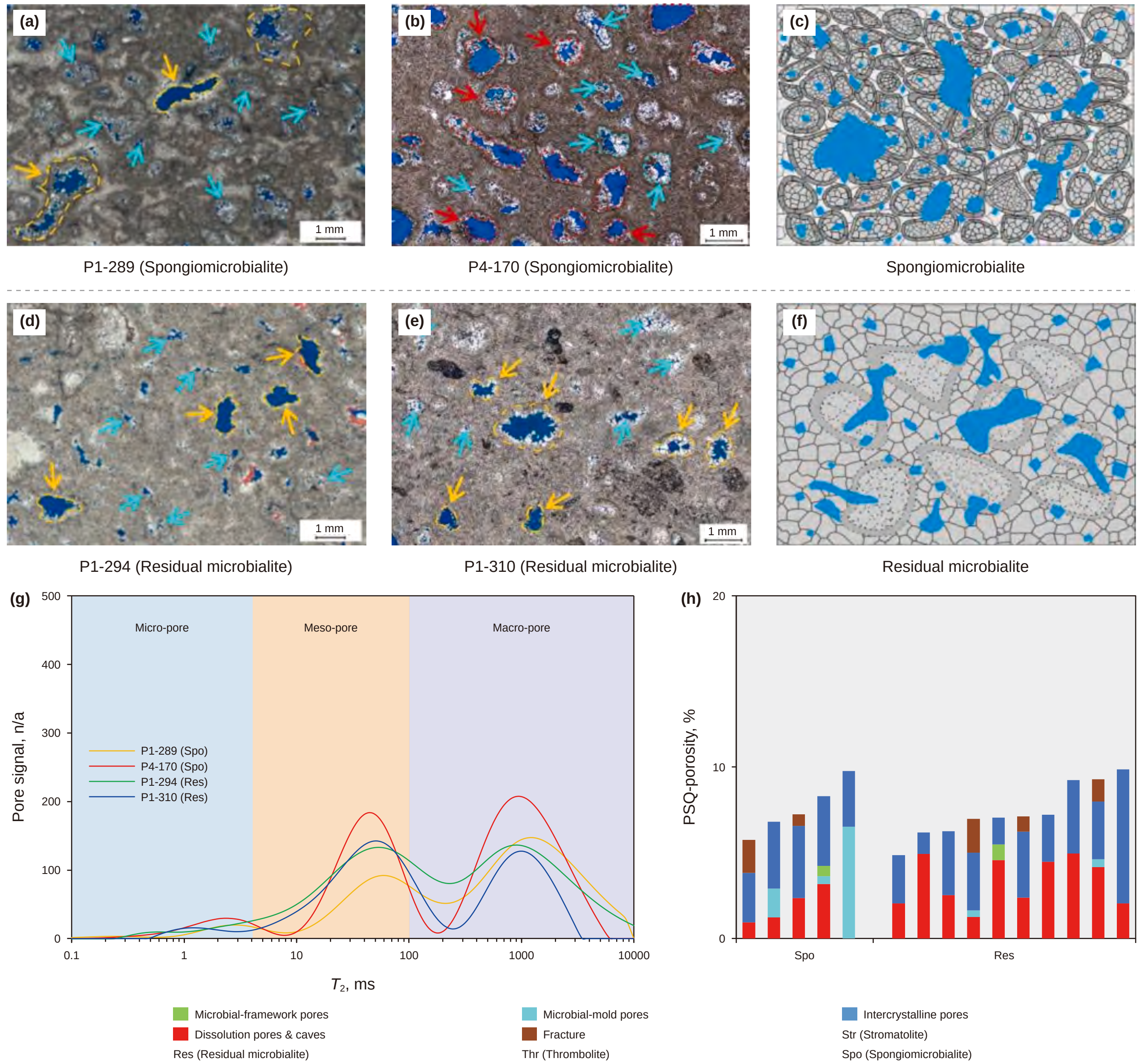

Fig. 11. Comparison of pore morphology, T_2 curves, and PSQ statistics for DPT microbial dolomite. (**a**) Pore morphology in spongiomicrobialite: casting sheet image of P1-289. (**b**) Pore morphology in spongiomicrobialite: casting sheet image of P4-170. (**c**) Simplified diagram of the DPT pore system in spongiomicrobialite. (**d**) Pore morphology in residual microbialite: casting sheet image of P1-294. (**e**) Pore morphology in residual microbialite: casting sheet image of P1-310; (**f**) Simplified diagram of the DPT pore system in residual microbialite. (**g**) T_2 curves of DPT microbial dolomite. (**h**) PSQ-porosity of DPT microbial dolomite.

predominantly concentrated in the middle-upper parts of cycles, exhibiting well-developed compaction-resistant microbial frameworks with fewer micrite clots, and consequently higher primary porosity (Fig. 10(h)). In contrast, irregularly clustered thrombolites in the lower parts of cycles contain abundant irregular micrite clots and limited primary porosity. On the other hand, penecontemporaneous meteoric freshwater dissolution further amplifies vertical heterogeneity in microbial dolomite pore systems. In highstand systems tract (HST) platform-margin reef-shoal complexes (middle-upper parts of cycles), fabric-selective dissolution pores formed through meteoric freshwater leaching, whereas low-energy environments (lower parts of cycles) lack significant penecontemporaneous dissolution (Shen et al., 2015). Comparable documentation derives from Miocene microbial carbonates in southeastern Spain, where vertical stacking of distinct sedimentary sequences-comprising oolites, microbialites (thrombolites, stromatolites), bioclastic sands, and coralgal reefs-is governed by relative sea-level fluctuations (Lipinski et al., 2013).

5.3. *Preservation mechanisms of pore systems controlled by early dolomitization*

The Ediacaran period, a crucial transitional phase in geological history between the Proterozoic and Phanerozoic eras, was marked by seawater conditions featuring elevated temperatures, low oxygen levels, high palaeosalinity, a high Mg/Ca ratio, increased pH, and comparatively low sulfate concentrations (Wood et al., 2017; Hood and Wallace, 2018; Mills et al., 2019; Zhang et al., 2020). Microbial

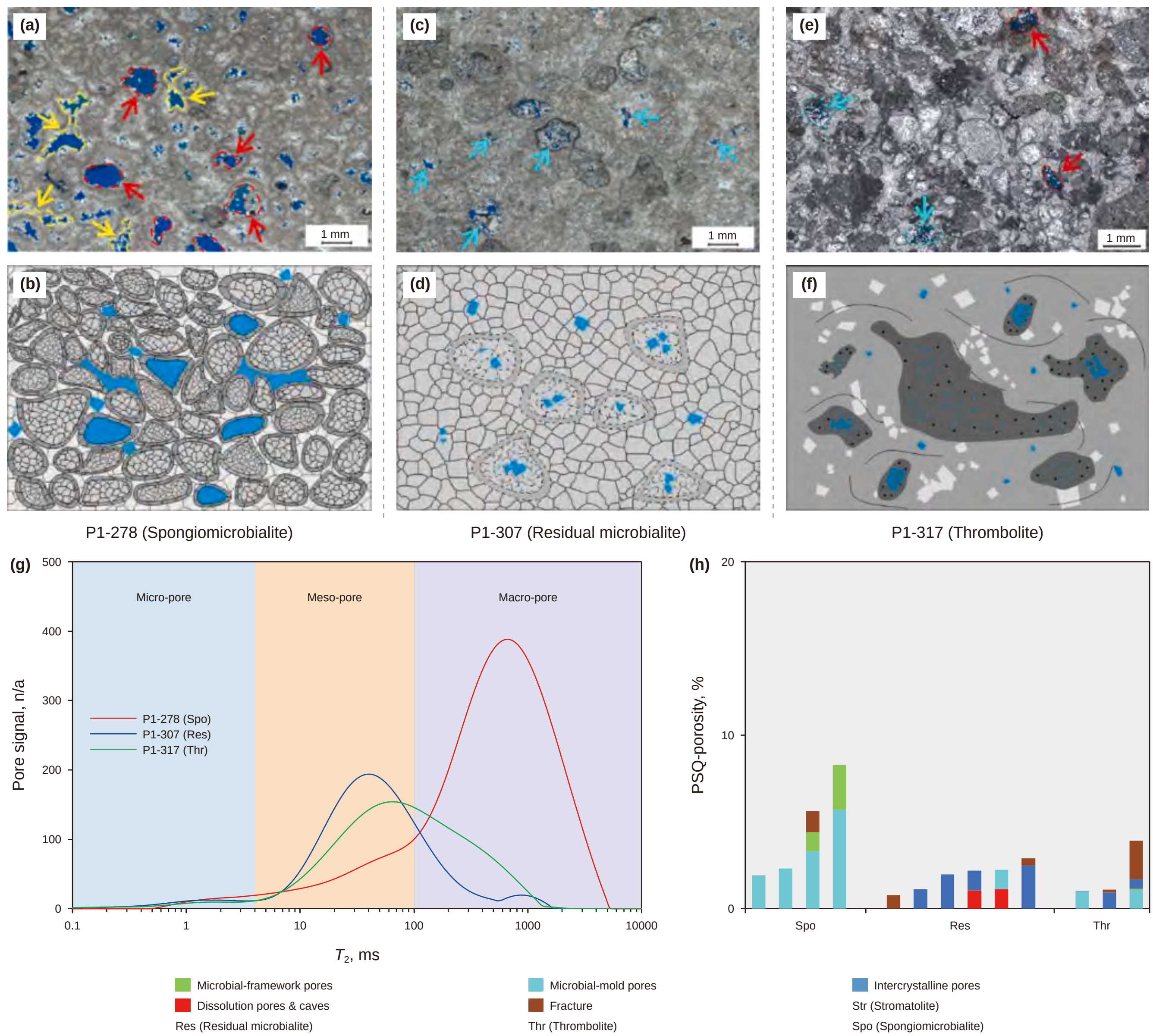

Fig. 12. Comparison of pore morphology, T_2 curves, and PSQ statistics for SPT microbial dolomite. (**a**) Pore morphology in spongiomicrobialite: casting sheet image of P1-278. (**b**) Simplified diagram of the SPT pore system in spongiomicrobialite. (**c**) Pore morphology in residual microbialite: casting sheet image of P1-307. (**d**) Simplified diagram of the SPT pore system in residual microbialite. (**e**) Pore morphology in thrombolite: casting sheet image of P1-317. (**f**) Simplified diagram of the SPT pore system in thrombolite. (**g**) T_2 curves of SPT microbial dolomite. (**h**) PSQ-porosity of SPT microbial dolomite.

activity likely played a significant role in facilitating early dolomitization within this unique "dolomite sea" environment (Wang et al., 2020; Zhao et al., 2021; Zhang et al., 2022). This dolomite exhibits dumbbell-shaped, spherical, and irregular grain morphologies, with diameters ranging from several nanometers to a few micrometers (Fig. 15(a)). These grains are typically distributed in mat-like structures or clusters (Fig. 15(b)). Scanning electron microscopy revealed tiny filamentous structures, suspected to be mineralized microbial fabric such as extracellular polymeric substances (EPS), within the microbial dolomite samples (Fig. 15(c)–(d)). The organic molecules in EPS contain numerous negatively charged functional groups that efficiently adsorb cations such as Ca^{2+} and Mg^{2+}. These groups also serve as effective nucleation sites, thereby promoting dolomite formation (Dupraz et al., 2009; Braissant et al., 2009; Petrash et al., 2017; Xiao et al., 2024).

Dolomitization processes in the Qigebrak Formation were predominantly completed during the penecontemporaneous period, as evidenced by recent clumped isotope ($T_{\Delta 47}$) and U-Pb dating (Chen et al., 2023). These early-formed dolomites generally demonstrate enhanced compaction strength and chemical stability relative to limestone (Schmoker and Halley, 1982; Ehrenberg et al., 2006), indicating that early dolomitization may improve the resistance of microbial dolomites to compaction enhances their chemical stability and resistance to compaction. The dark laminations of stromatolite and the sponge-like frameworks serve as robust, compaction-resistant structures (Fig. 10(b) and (d)). Consequently,high-frequency sedimentary cycles, penecontemporaneous dissolution, and early dolomitization jointly control the vertical differentiation and preservation of early pore systems in microbial dolomites.

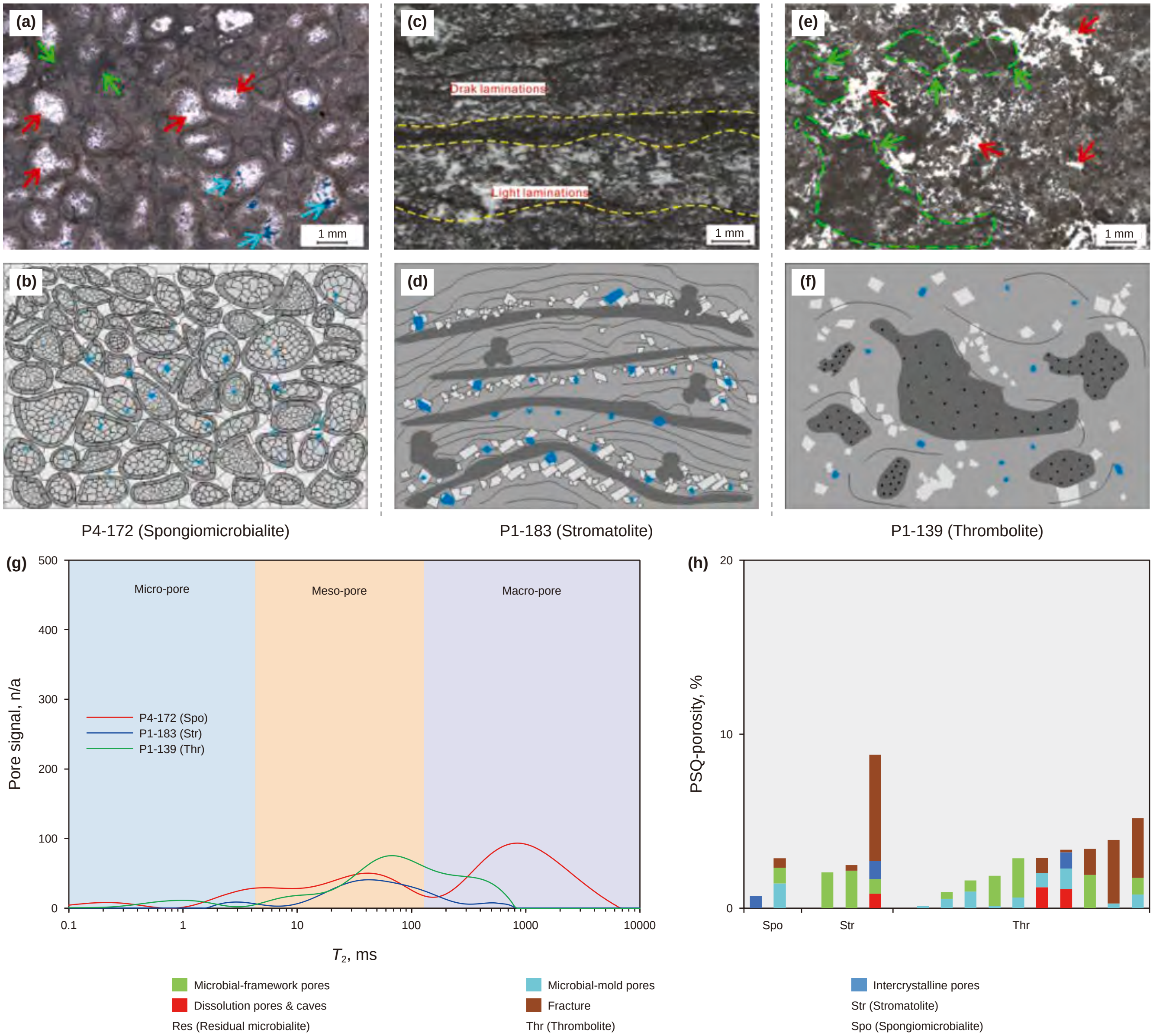

Fig. 13. Comparison of pore morphology, T_2 curves, and PSQ statistics for MLT microbial dolomite. (**a**) Pore morphology in spongiomicrobialite: casting sheet image of P4-172. (**b**) Simplified diagram of the MLT pore system in spongiomicrobialite. (**c**) Pore morphology in stromatolite: casting sheet image of P1-183. (**d**) Simplified diagram of the MLT pore system in stromatolite. (**e**) Pore morphology in thrombolite: casting sheet image of P1-139. (**f**) Simplified diagram of the MLT pore system in thrombolite. (**g**) T_2 curves of MLT microbial dolomite; (**h**) PSQ-porosity of MLT microbial dolomite.

5.4. Effects of sedimentary and diagenetic processes on microbial dolomite pore system

Porosity and permeability distributions reveal nuanced changes in pore size and connectivity that are intricately linked to microbial rock depositional structures (Qu et al., 2018). They also reflect the subtle effects of microbial depositional environments and diagenetic conditions on the pore system (Brigaud et al., 2014; Zhu et al., 2020b; Armelenti et al., 2021; Abdlmutalib et al., 2022; Hamd et al., 2022; Rossoni et al., 2024). Influenced by the depositional environment, microbial dolomites exhibit various lithostructural features, encompassing histocompositional type, grain separability, mud content, and others (Zhang et al., 2022; Vescogni et al., 2022; Abdel et al., 2023). Furthermore, the depositional environment significantly influences lithofacies distribution patterns, sedimentary paleomorphology and microbial activities (Mettraux et al., 2015; Suarez et al., 2019). The interplay of these factors leads to considerable variation in the morphology, abundance, and spatial distribution of primary pores within microbial dolomites (Qu et al., 2018; Zhai et al., 2023).

Spongiomicrobialite and wavy stromatolite are inclined to form in the upper and middle sections of the cycles, while thrombolite and flat laminite stromatolite are more prevalent in the lower regions (Fig. (2)). The spongiomicrobialite sample (No. P4-159), derived from a high-energy depositional environment in the upper-middle part of the cycles, is characterized by a rich diversity of microbial mold pore structures (Fig. (6)). The nuclear magnetic resonance (NMR) T_2 curves of this sample displays typical MHT-type features (Fig. 10(g)). In contrast, the laminite stromatolite sample (No. P1-183), formed in a low-energy depositional environment, exhibits significantly limited primary pore development (Fig. (6)) and presents MLT-type features in its T_2 curves (Fig. (13)).

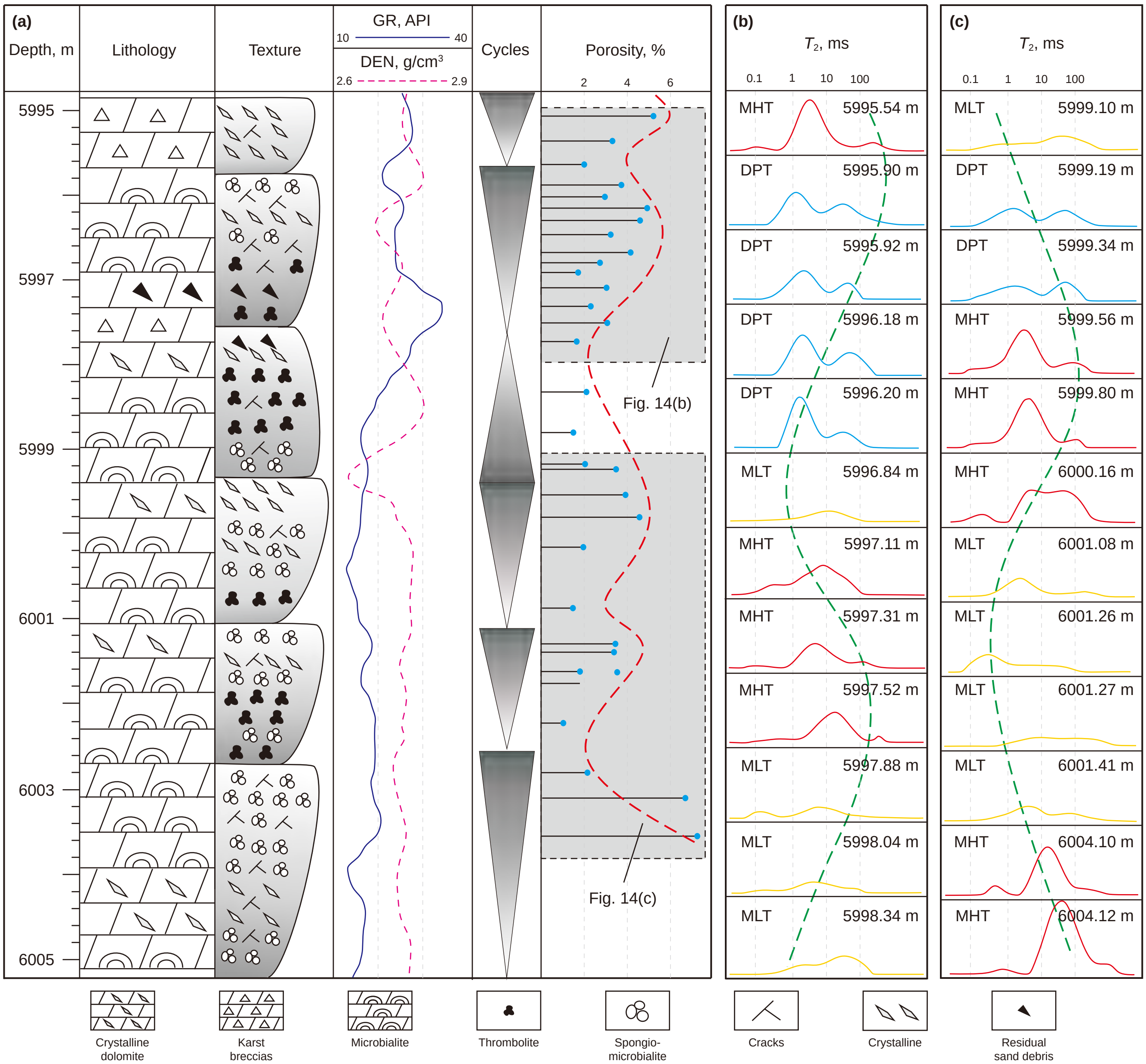

Fig. 14. Vertical distribution characteristics of NMR T_2 curves of dolomite in the Qigebrak Formation of Well QT1. (**a**) Comprehensive core histogram of dolomite in the Qigebrak Formation of Well QT1 (depth: 5995–6005 m) (Chen et al., 2023). (**b**), (**c**) Vertical distribution of different types of NMR T_2 curves.

Comparable case studies have been reported from the Upper Permian Zechstein Formation in northeastern England. Laminite stromatolites and thrombolites, which formed in low-energy intertidal (lagoon) and supratidal settings, exhibit poor porosity and permeability. In contrast, oolitic dolostones and wavy stromatolites formed in high energy shallow subtidal environments and serve as high-quality hydrocarbon reservoirs (Słowakiewicz et al., 2013).

The reef sedimentary system, situated in the upper part of the highstand system tract (HST) quasi-sequence group, is susceptible to atmospheric freshwater leaching, which results in the formation of fabric-selective pores (Lu et al., 2018; Wang et al., 2023). Periodic declines in sea level result in brief exposures of the sedimentary system, which intensifies erosion (Fig. (16)). The subsequent periodic exposure and dissolution drive the cyclic changes observed in the vertical distribution of microbial dolomite pores (Shen et al., 2015; Chen et al., 2023). The primary pores in MHT spongiomicrobialite and stromatolite are likely enlarged further by dissolution under these conditions.

The Neoproterozoic Ediacaran microbial dolomites underwent significant changes in their pore systems due to intricate, multiphase diagenetic fluid alteration processes (Yan et al., 2019; Yang et al., 2020b; Chen et al., 2020; Jin et al., 2025). The pathways of diagenetic fluid flow and the progression of diagenetic evolution ultimately govern the distributional characteristics of microbial dolomite pores. This factor significantly influences the formation of most DPT pore systems and a subset of MHT pore systems. For example, samples P1-294 and P1-310 both underwent significant recrystallization processes and experienced strong dissolution effects (Fig. 11(d) and (e)). Fig. (16) illustrates the differential diagenetic evolution of the pore system in the restored microbial dolomites of the Qigebrak Formation.

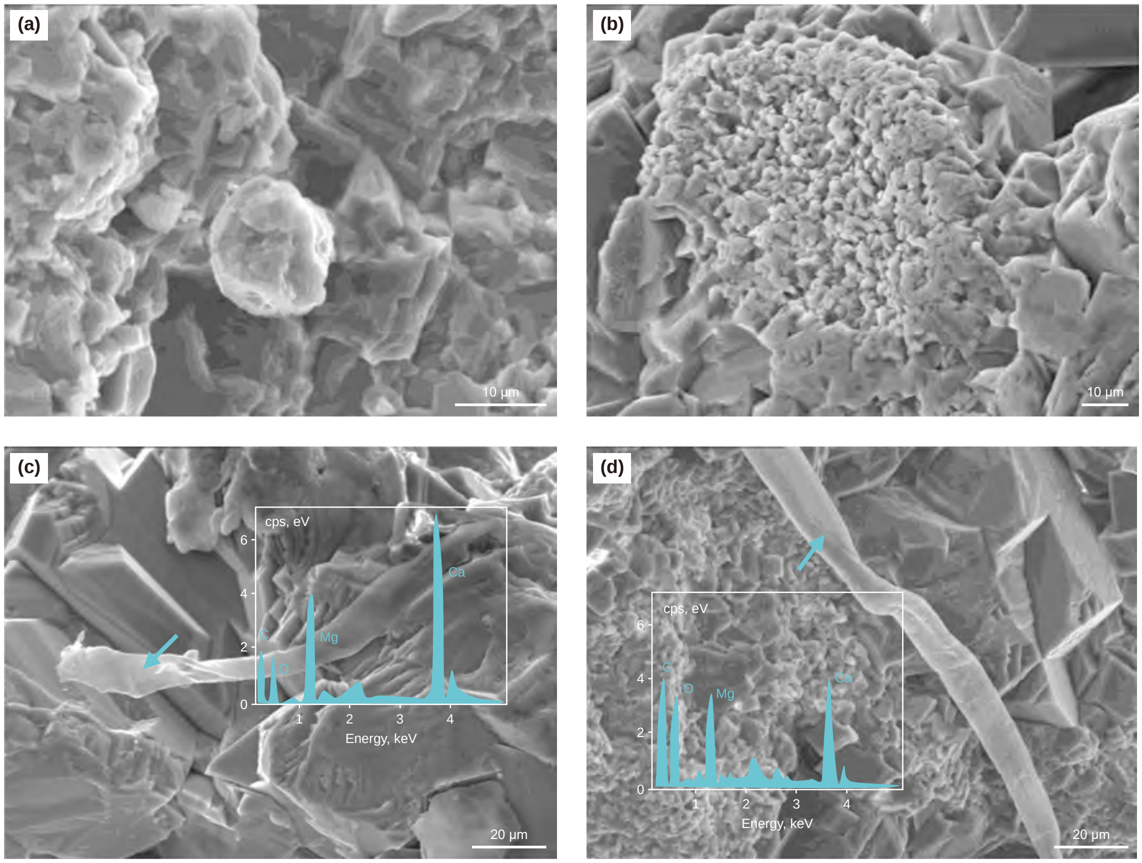

Fig. 15. Scanning electron microscope (SEM) images of microbial dolomite from the Qigebrak Formation, sampled at the Linkuanggou outcrop. (**a**) SEM image of spherical dolomite grains. (**b**) Microbial dolomites arranged in mat-like structures. (**c**), (**d**) SEM images of extracellular polymeric substances (EPS) with energy-dispersive spectroscopy (EDS) analysis identifying the elemental composition at the indicated positions (blue dots).

The early dolomitization was initiated by mesohaline seawater reflux seepage during the penecontemporaneous period (Zhao et al., 2024). Dolomitization of the Qigebrak Formation occurred during the penecontemporaneous period (Zheng et al., 2021a, 2021b), with early dolomitization favoring the preservation of primary porosity. Previous geochemical data have well supported this perspective. The clumped isotope temperatures ($T_{\Delta 47}$) of the microbial dolomite matrix are approximately 51 °C (Chen et al., 2023). The carbon and oxygen isotope values ($\delta^{18}O_{VPDB}$, −5.6‰ to −3.1‰, average = −4.4‰; $\delta^{13}C_{VPDB}$, 2.3‰–4.3‰, average = 3.3‰) fall within the range of Ediacaran seawater (Tang et al., 2022). The rare earth element distribution patterns resemble those of seawater, showing super-chondritic Y/Ho ratios and light rare earth element (LREE) depletion (Zhao et al., 2024).

Cementation during the shallow burial period caused the first significant reduction in the primary pores of the microbial dolomites in the Qigebrak Formation (Chen et al., 2023). Fibrous dolomite cements precipitated from marine fluid in the eodiagenetic stage, partially occluding minor pore spaces (Yang et al., 2020a). Granular dolomite cements by confined pore fluids during the meso-shallow burial stage significantly occluded the majority of early-stage reservoir spaces (Yang et al., 2020a; Chen et al., 2023). These granular dolomite cements have relatively high fluid inclusion homogenization temperatures (80 °C–138 °C) and negative oxygen isotope (−10.7‰–7.6‰) (Zhao et al., 2024). PSQ analysis indicates that the average cement content in the pores of spongiomicrobialite, stromatolite, and thrombolite was 10.67%, 19.66%, and 15.32%, respectively (Table 1). Notably, the stromatolite sample P3-153 contained up to 33.47% collodion cement (Fig. (6)).

The Keping tectonic event, happening at the close of the Ediacaran Epoch, was the chief factor in the creation of widespread dissolution caves in the microbial dolomite. This karstic process led to the development of a series of weathered crusts atop the Qigebrak Formation (Wu et al., 2021; Zhang et al., 2024). The layer spanning from 60 to 80 m below the unconformity undergoes varying degrees of dissolution due to freshwater infiltration (Chen et al., 2020). Additionally, the primary pores experience subsequent further dissolution. The $\delta^{13}C$ and $\delta^{18}O$ values of dolomite in the upper part of the Qigebrak Formation under strong meteoric dissolution have a simultaneous negative shift ($\delta^{13}C_{VPDB,}$ 1‰–2‰; $\delta^{18}O_{VPDB,}$ −9‰ to −7‰), and there is a positive correlation between $\delta^{13}C$ and $\delta^{18}O$ (Chen et al., 2023). Hence, MHT microbial dolomite not only exhibits abundant microbial-framework pores and microbial mold pores, but also prominently features non-fabric selective pores (Fig. (8)).

After undergoing significant diagenetic modification, the microbial dolomite experienced recrystallization, oil and gas filling, as well as compaction and dissolution at deeper stratigraphic levels. This process led to the destruction of the original sedimentary structure, while retaining intercrystalline pores and some dissolution pores. It formed residual microbialite of the MHT or DPT type. However, in the case of microbial dolomites with poorly developed primary porosity, the MLT microbial dolomite is formed in a relatively confined diagenetic environment, where stratigraphic fluid activity is limited and the original sedimentary structure is well preserved (Fig. (13)).

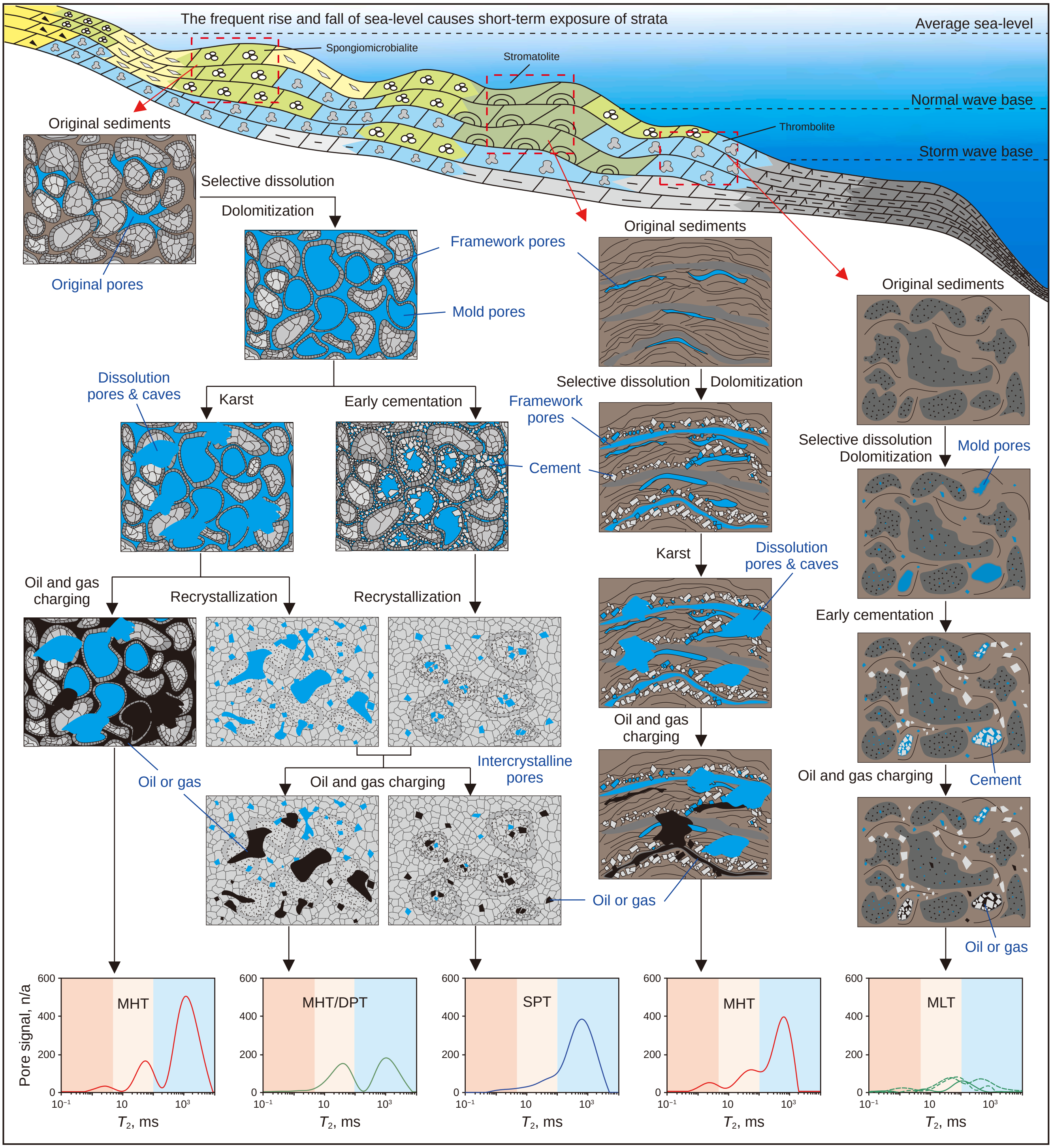

Fig. 16. Schematic illustration showing the distribution pattern of microbial dolomites and pore space evolution recognized in the studied reservoir of the Ediacaran. Microbial dolomite sedimentary distribution pattern according to Chen et al. (2023).

6. Conclusions

1. The key processes governing the formation and preservation of microbial dolomite pore systems have been systematically deciphered. Through systematic NMR T_2 curve analysis, a robust classification framework was established to differentiate four distinct pore architectures: (1) microbial framework-hosted (MHT) systems exhibiting high porosity with multi-modal primary pores, (2) diagenetically-processed (DPT) systems dominated by intercrystalline and dissolution porosity, (3) single-pore-type (SPT) systems preserving isolated primary pores, and (4) matrix-limited (MLT) systems showing under-developed porosity networks (<2% porosity).
2. The vertical differentiation and preservation of early-stage pore systems in microbial dolomites are collectively governed by microbial dolomite construction under high-frequency

depositional cycles (controlling primary fabric heterogeneity), penecontemporaneous short-term dissolution (enhancing pore connectivity), and early dolomitization (improving pore preservation through enhanced compaction resistance during initial burial).
3. Distinct variations in pore system characteristics and diagenetic evolution are evident among different microbial dolomite types. The pore system formation in the Qigebrak Formation underscores the influence of elevated sedimentary environments on primary porosity development, while diagenetic fluid alterations contribute to secondary pore formation and the transition to MHT or DPT systems. In contrast, SPT and MLT systems typically retain their original structure due to limited fluid flow.

CRediT authorship contribution statement

Xu-Dong Chen: Writing – original draft, Investigation, Formal analysis, Data curation, Conceptualization. **Qi-Lu Xu:** Writing – review & editing, Supervision, Investigation, Funding acquisition. **Fang Hao:** Supervision, Funding acquisition. **Guo Yang:** Resources, Conceptualization. **Ping Wang:** Resources, Formal analysis. **Fei-Fei Yuan:** Writing – review & editing. **Xin-Le Li:** Writing – review & editing. **Jin-Qiang Tian:** Supervision, Conceptualization. **Guang-Wei Wang:** Supervision, Conceptualization.

Conflict of interest statement

The authors declare that there are no conflicts of interest regarding the publication of this manuscript. All authors have disclosed any potential financial or personal relationships that could influence the research presented in this paper. This includes any affiliations, funding sources, or financial interests that may be perceived as influencing the objectivity or integrity of the work.

Acknowledgements

This study is supported by the National Natural Science Foundation of China (Grant Nos. 42272154, 41821002), the Fundamental Research Funds for the Central Universities (Grant No. 24CX02008A), and the Fund of State Key Laboratory of Deep Oil and Gas, China University of Petroleum (East China). This study is also supported by the program of PetroChina Tarim Oilfield Company (Grant No. 671024115048).

References

Abdel, F.Z.A., Sehsah, H., Rogers, B.C.C., 2023. Ediacaran microbial mats and microbially induced sedimentary structures in lacustrine deposits, Arabo-Nubian shield, Egypt. Sediment. Geol. 457, 106517. https://doi.org/10.1016/j.sedgeo.2023.106517.
Abdlmutalib, A.J., Ayranci, K., Yassin, M.A., Hussaini, S.R., Abdullatif, O.A., Humphrey, J.D., 2022. Impact of sedimentary fabrics on small-scale permeability variations within fine-grained sediments: Early Silurian Qusaiba member, Northern Saudi Arabia. Mar. Petrol. Geol. 139, 105607. https://doi.org/10.1016/j.marpetgeo.2022.105607.
Armelenti, G., Goldberg, K., Alvarenga, R., Kuchle, J., Amarante, F.B., Scherer, C.M.S., Bastos, A.C., Conceição, J.C., Alves, J.L.D., De Ros, L.F., 2021. Depositional and diagenetic impacts on the porosity of post-salt carbonate reservoirs of southern Campos Basin, southeastern Brazilian margin. J. South Am. Earth Sci. 112, 103566. https://doi.org/10.1016/j.jsames.2021.103566.
Braissant, O., Decho, A.W., Przekop, K.M., Gallagher, K.L., Glunk, C., Dupraz, C., Visscher, P.T., 2009. Characteristics and turnover of exopolymeric substances in a hypersaline microbial mat. FEMS Microbiol. Ecol. 67 (2), 293–307. https://doi.org/10.1111/j.1574-6941.2008.00614.x.
Brigaud, B., Vincent, B., Durlet, C., Deconinck, J.F., Jobard, E., Pickard, N., Yven, B., Landrein, P., 2014. Characterization and origin of permeability-porosity heterogeneity in shallow-marine carbonates: From core scale to 3D reservoir dimension (Middle Jurassic, Paris Basin, France). Mar. Petrol. Geol. 57, 631–651. https://doi.org/10.1016/j.marpetgeo.2014.07.004.
Chen, L.P., Zhang, H., Cai, Z.X., Cong, F.Y., Huang, S., Tang, P., 2020. Characteristics and formation mechanisms of the unconformity-related paleokarst reservoirs in the Upper Sinian, Northwestern Tarim Basin, China. Mar. Petrol. Geol. 120, 104559. https://doi.org/10.1016/j.marpetgeo.2020.104559.
Chen, X.D., Xu, Q.L., Hao, F., Chen, Y.Q., Yi, Y., Hu, F.J., Wang, X.X., Tian, J.Q., Wang, G.W., 2023. Dolomite reservoir formation and diagenesis evolution of the Upper Ediacaran Qigebrak Formation in the Tabei area, Tarim Basin. Sci. China Earth Sci. 66 (10), 2311–2331. https://doi.org/10.1007/s11430-022-1103-4.
Chen, Y.C., Yang, G., Tian, H.N., Chen, B., Yi, Y., Li, B.H., 2024. Ediacaran stratigraphic succession and sedimentary evolution of the Tarim Craton. J. Stratigr. 48 (1), 17–41. https://doi.org/10.19839/j.cnki.dcxzz.2024.0001 (in Chinese).
Chen, Y.N., Shen, A.J., Pan, L.Y., Zhang, J., Wang, X.F., 2017. Features, origin and distribution of microbial dolomite reservoirs: A case study of 4th member of Sinian Dengying Formation in Sichuan Basin, SW China. Petrol. Explor. Dev. 44 (5), 704–715. https://doi.org/10.11698/PED.2017.05.05 (in Chinese).
Dupraz, C., Reid, R.P., Braissant, O., Decho, A.W., Norman, R.S., Visscher, P.T., 2009. Processes of carbonate precipitation in modern microbial mats. Earth Sci. Rev. 96, 141–162. https://doi.org/10.1016/j.earscirev.2008.10.005.
Ehrenberg, S.N., Eberli, G.P., Keramati, M., Moallemi, S.A., 2006. Porosity-permeability relationships in interlayered limestone-dolostone reservoirs. AAPG Bull. 90, 91–114. https://doi.org/10.1306/08100505087.
Ehrenberg, S.N., Walderhaug, O., Bjørlykke, K., 2012. Carbonate porosity creation by mesogenetic dissolution: Reality or illusion. AAPG Bull. 97 (2), 217–233. https://doi.org/10.1306/07111212045.
Grotzinger, J., Al-Rawahi, Z., 2014. Depositional facies and platform architecture of microbialite-dominated carbonate reservoirs, Ediacaran-Cambrian Ara group, Sultanate of Oman. AAPG Bull. 98 (8), 1453–1494. https://doi.org/10.1306/02271412063.
Guan, S.W., Wu, L., Ren, R., Zhu, G.Y., Peng, C.Q., Zhao, W.T., Li, J., 2017. Distribution and petroleum prospect of Precambrian rifts in the main cratons, China. Acta Petrol. Sin. 38 (1), 9–22. https://doi.org/10.7623/syxb201701002 (in Chinese).
Guo, X.S., Hu, Z.Q., Li, S.J., Zheng, L.J., Zhu, D.Y., Liu, J.L., Shen, B.J., Du, W., Yu, L.J., Liu, Z.Q., Huangfu, R.L., 2023. Progress and prospect of natural gas exploration and research in deep and ultra-deep strata. Pet. Sci. Bull. 8 (4), 461–474. https://doi.org/10.3969/j.issn.2096-1693.2023.04.035 (in Chinese).
Haddad, S.A., Mancini, E.A., 2013. Reservoir characterization, modeling, and evaluation of Upper Jurassic Smackover microbial carbonate and associated facies in little cedar creek field, southwest Alabama, eastern Gulf coastal plain of the United States. AAPG Bull. 97 (11), 2059–2083. https://doi.org/10.1306/07081312187.
Hamd, J., Cerepi, A., Swennen, R., Loisy, C., Galaup, S., Pigot, L., 2022. Sedimentary and diagenetic effects on reservoir properties of upper Cretaceous Ionian Basin and Kruja platform carbonates, Albania. Mar. Petrol. Geol. 138, 105549. https://doi.org/10.1016/j.marpetgeo.2022.105549.
Hao, F., 2022. Enrichment mechanism and prospects of deep oil and gas. Acta Geol. Sin. 96 (3), 742–756. https://doi.org/10.1111/1755-6724.14961.
Hao, F., Zhang, X.F., Wang, C.W., Li, P., Guo, T.L., Zou, H.Y., Zhu, Y.M., Liu, J.Z., Cai, Z.X., 2015. The fate of CO_2 derived from thermochemical sulfate reduction (TSR) and the effect of TSR on carbonate porosity and permeability, Sichuan Basin, China. Earth Sci. Rev. 141, 154–177. https://doi.org/10.1016/j.earscirev.2014.12.001.
Hood, A.V.S., Wallace, M.W., 2018. Neoproterozoic marine carbonates and their paleoceanographic significance. Global Planet. Change 160, 28–45. https://doi.org/10.1016/j.gloplacha.2017.11.006.
Hu, A.P., Shen, A.J., Zheng, J.F., Wang, X., Wang, X.F., 2021. The classification, facies and sedimentary models of microbialites. Mar. Orig. Pet. Geol. 26 (1), 1–15. https://doi.org/10.3969/j.issn.1672-9854.2021.01.001 (in Chinese).
Hu, Y.J., Cai, C.F., Li, Y., Liu, D.W., Wei, T.Y., Wang, D.W., Jiang, L., Ma, R.T., Shi, S.Y., Immenhauser, A., 2023. Sedimentary and diagenetic archive of a deeply buried, upper Ediacaran microbialite reservoir, Southwestern China. AAPG Bull. 107 (3), 387–412. https://doi.org/10.1306/08232221122.
Huang, W.W., Zhang, L.L., Zhu, D.C., Liu, L., Li, X.W., Xie, J.C., Wang, Q., Chi, H.Y., 2025. Age constraints on the Ediacaran carbonate carbon isotope excursions in the Tarim Block: Evidence from in situ U-Pb dating of dolostone. Precambr. Res. 418, 107691. https://doi.org/10.1016/j.precamres.2025.107691.
Jin, X., Song, J.M., Liu, S.G., Wang, B., Yang, D., Li, Z.W., Tian, L.Z., Deng, H.S., Ren, S., Xue, J.M., Guo, J.X., Zhang, Z.Y., Shao, X.P., 2025. Coupled effects of paleofluid evolution on ultra-deep microbialite reservoir modification: A case study of the upper Ediacaran Deng-2 member with in the Penglai area of Central Sichuan Basin, SW China. Pet. Sci. 22 (2), 527–545. https://doi.org/10.1016/j.petsci.2024.10.001.
Lai, J., Wang, S., Zhang, C.S., Wang, G.W., Song, Q.Q., Chen, X., Yang, K.F., Yuan, C.J., 2020. Spectrum of pore types and networks in the deep Cambrian to Lower Ordovician dolostones in Tarim Basin, China. Mar. Petrol. Geol. 112, 104081. https://doi.org/10.1016/j.marpetgeo.2019.104081.
Li, C.W., Liu, K.Y., Liu, J.L., 2023. A petroliferous Ediacaran microbial-dominated carbonate reservoir plays in the central Sichuan Basin, China: Characteristics and diagenetic evolution. Precambr. Res. 384, 106937. https://doi.org/10.1016/j.precamres.2022.106937.
Li, P.W., Luo, P., Song, J.M., Jin, T.F., Wang, G.Q., 2015b. Characteristics and main controlling factors of upper Sinian-Lower Cambrian in the northwestern margin of Tarim Basin. Acta Petrol. Sin. 36 (9), 1074–1089. https://doi.org/10.7623/syxb201509005 (in Chinese).

Li, P.W., Luo, P., Chen, M., Song, J.M., Jin, T.F., Wang, G.Q., 2015a. Characteristics and origin of the upper Sinian microbial carbonate reservoirs at the northwestern margin of Tarim Basin. Oil Gas Geol. 36 (3), 416–428. https://doi.org/10.11743/ogg20150310 (in Chinese).

Lipinski, C.J., Franseen, E.K., Goldstein, R.H., 2013. Reservoir analog model for oolite-microbialite sequences, Miocene terminal carbonate complex, Spain. AAPG Bull. 97 (11), 2035–2057. https://doi.org/10.1306/06261312182.

Liu, Z.S., Liu, D.M., Cai, Y.D., Yao, Y.B., Pan, Z.J., Zhou, Y.F., 2020. Application of nuclear magnetic resonance (NMR) in coalbed methane and shale reservoirs: A review. Int. J. Coal Geol. 218, 103261. https://doi.org/10.1016/j.coal.2019.103261.

Loucks, R.G., 2018. Domal, thrombolitic, microbialite biostromes and associated lithofacies in the upper Albian devils river trend along the northern, high-energy margin of the Maverick Basin. Sediment. Geol. 371, 75–88. https://doi.org/10.1016/j.sedgeo.2018.04.010.

Lu, C.J., Liu, Z., Tian, H.Q., Liu, M.J., Lin, J.H., Wang, Y., Yang, X.G., 2018. An eogenetic paleokarst model controlled by multi-level sea-level: A case study of Shilongdong Formation in lower Cambrian, from the west Hubei and the east Chongqing to the west Hunan and Hubei, SW China. J. China Univ. Min. Technol. 47 (5), 1055–1066. https://doi.org/10.13247/j.cnki.jcumt.000846 (in Chinese).

Luo, P., Wang, S., Li, P.W., Song, J.M., Jin, T.F., Wang, G.Q., Yang, S.S., 2013. Review and prospectives of microbial carbonate reservoirs. Acta Sedimentol. Sin. 31 (5), 807–823. https://doi.org/10.14027/j.cnki.cjxb.2013.05.005 (in Chinese).

Ma, Y.S., Cai, X.Y., Li, M.W., Li, H.L., Zhu, D.Y., Qiu, N.S., Pang, X.Q., Zeng, D.Q., Kang, Z.J., Ma, A.L., Shi, K.B., Zhang, J.T., 2024. Research advances on the mechanisms of reservoir formation and hydrocarbon accumulation and the oil and gas development methods of deep and ultra-deep marine carbonates. Petrol. Explor. Dev. 51 (4), 692–707. https://doi.org/10.11698/PED.20240072 (in Chinese).

Mei, M.X., 2007. Discussion on advances of microbial carbonates from the terminological change of thrombolites. Geol. Sci. Technol. Inf. 26 (6), 1–9 (in Chinese).

Mettraux, M., Homewood, P., Anjos, C.D., Erthal, M., Lima, R., Matsuda, N., Souza, A., Balushi, A., 2015. Microbial communities and their primary to early diagenetic mineral phases; the record from Neoproterozoic microbialites of Qarn Alam, Oman. Geol. Soc. Lond. Spec. Public. 418, 123–154. https://doi.org/10.1144/sp418.5.

Mills, B.J.W., Krause, A.J., Scotese, C.R., Hill, D.J., Shields, G.A., Lenton, T.M., 2019. Modelling the long-term carbon cycle, atmospheric CO_2, and earth surface temperature from late Neoproterozoic to present day. Gondwana Res. 67, 172–186. https://doi.org/10.1016/j.gr.2018.12.001.

Petrash, D.A., Bialik, O.M., Bontognali, T.R.R., Vasconcelos, C., Roberts, J.A., McKenzie, J.A., Konhauser, K.O., 2017. Microbially catalyzed dolomite formation: From near-surface to burial. Earth Sci. Rev. 171, 558582. https://doi.org/10.1016/j.earscirev.2017.06.015.

Qu, H.J., Li, P., Dong, Y.P., Yang, B., Chen, S., Han, X., Wang, K., He, M., 2020. Development and distribution rules of the main Neoproterozoic source and reservoir strata in the Yangtze block, Southern China. Precambr. Res. 350, 105915. https://doi.org/10.1016/j.precamres.2020.105915.

Qu, H.Z., Zhou, Z.K., Zhang, Y.F., Chen, W., Zhang, Z.H., Luo, X.S., Ma, C., Tan, F., Zhu, Y.H., 2018. Research progress of porosity in microbial carbonates. Acta Sedimentol. Sin. 36 (4), 651–663. https://doi.org/10.14027/j.issn.1000-0550.2018.055 (in Chinese).

Rezende, M.F., Tonietto, S.N., Pope, M.C., 2013. Three-dimensional pore connectivity evaluation in a Holocene and Jurassic microbialite buildup. AAPG Bull. 97 (11), 2085–2101. https://doi.org/10.1306/05141312171.

Rossoni, R.B., Porcher, C.C., Koester, E., Sobiesiak, J.S., Silva, L.A.C., Mexias, A.S., Gomes, M.E.B., Ramnani, C.W., Ros, L.F.D., 2024. The role of compaction in the diagenetic evolution of Pre-salt Aptian deposits of Santos Basin, Brazil. Sediment. Geol. 466, 106650. https://doi.org/10.1016/j.sedgeo.2024.106650.

Schmoker, J.W., Halley, R.B., 1982. Carbonate porosity versus depth: A predictable relation for south Florida. AAPG Bull. 66, 2561–2570. https://doi.org/10.1306/03B5AC73-16D1-11D7-8645000102C1865D.

Schröder, S., Grotzinger, J.P., Amthor, J.E., Matter, A., 2005. Carbonate deposition and hydrocarbon reservoir development at the Precambrian-Cambrian boundary: The Ara group in South Oman. Sediment. Geol. 180, 1–28. https://doi.org/10.1016/j.sedgeo.2005.07.002.

Shen, A.J., Hu, A.P., Qiao, Z.F., Zheng, J.F., She, M., Pan, L.Y., 2024. Development and preservation mechanism of deep and ultra-deep carbonate reservoirs. Sci. China Earth Sci. 67 (11), 3367–3385. https://doi.org/10.1007/s11430-023-1417-8.

Shen, A.J., Hu, A.P., Zhang, J., Wang, X.F., Wang, H., 2022. “Three-factor” driven microbial carbonate reservoirs and their distribution. Oil Gas Geol. 43 (3), 582–596. https://doi.org/10.11741/ogg20220308 (in Chinese).

Shen, A.J., Zhao, W.Z., Hu, A.P., She, M., Chen, Y.N., Wang, X.F., 2015. Major factors controlling the development of marine carbonate reservoirs. Petrol. Explor. Dev. 42 (5), 597–608. https://doi.org/10.11698/PED.2015.0501.

Shi, K.B., Liu, B., Jiang, W.M., Luo, Q.Q., Gao, X.Q., 2018. Nanhua-Sinian tectono-sedimentary framework of Tarim Basin, NW China. Oil Gas Geol. 39, 862–877. https://doi.org/10.11743/ogg20180502 (in Chinese).

Siahi, M., Hofmmann, A., Hegner, E., Master, S., 2016. Sedimentology and facies analysis of Mesoarchaean stromatolitic carbonate rocks of the Pongola supergroup, South Africa. Precambr. Res. 278, 244–264. https://doi.org/10.1016/j.precamres.2016.03.004.

Słowakiewicz, M., Tucker, M.E., Pancost, R.D., Perri, E., Mawson, M., 2013. Upper Permian (Zechstein) microbialites: Supratidal through deep subtidal deposition, source rock, and reservoir potential. AAPG Bull. 97 (11), 1921–1936. https://doi.org/10.1306/06181312179.

Smodej, J., Reuning, L., Becker, S., Kukla, P.A., 2019. Micro- and nano-pores in intrasalt, microbialite-dominated carbonate reservoirs, Ara group, South-Oman salt basin. Mar. Petrol. Geol. 104, 389–403. https://doi.org/10.1016/j.marpetgeo.2019.03.036.

Song, J.M., Jin, X., Luo, Z., Liu, S.G., Liu, S.B., Ma, X.Z., Li, Z.W., Lu, X.S., Zhao, L.L., Li, K.R., Ren, J.X., Tian, L.Z., Deng, H.S., 2024. Depositional model of the member Deng-2 marginal microbial mound-bank complex of the Dengying Formation in the Southwestern Sichuan Basin, SW China: Implications for the Ediacaran microbial mound construction and hydrocarbon exploration. Pet. Sci. 21 (2), 806–822. https://doi.org/10.1016/j.petsci.2023.12.005.

Song, J.M., Luo, P., Yang, S.S., Yang, D., Zhou, C.M., Li, P.W., Zhai, X.F., 2014. Reservoirs of Lower Cambrian microbial carbonates, Tarim Basin, NW China. Petrol. Explor. Dev. 41 (4), 404–413+437. https://doi.org/10.11698/PED.2014.04.03 (in Chinese).

Suarez, G.P., Benito, M.I., Quijada, I.E., Mas, R., Campos, S.S., 2019. ‘Trapping and binding’: A review of the factors controlling the development of fossil agglutinated microbialites and their distribution in space and time. Earth Sci. Rev. 194, 182–215. https://doi.org/10.1016/j.earscirev.2019.05.007.

Tang, P., Chen, D.Z., Wang, Y.Z., Ding, Y., Shafeiy, E.M., Yang, B., 2022. Diagenesis of microbialite-dominated carbonates in the upper Ediacaran Qigebrak Formation, NW Tarim Basin, China: Implications for reservoir development. Mar. Petrol. Geol. 136, 105476. https://doi.org/10.1016/j.marpetgeo.2021.105476.

Vescogni, A., Guido, A., Cipriani, A., Gennari, R., Lugli, F., Lugli, S., Manzi, V., Reghizzi, M., Roveri, M., 2022. Palaeoenvironmental setting and depositional model of upper Messinian microbialites of the Salento Peninsula (Southern Italy): A central mediterranean terminal carbonate complex. Paleogeogr. Paleoclimatol. Paleoecol. 595, 110970. https://doi.org/10.1016/j.palaeo.2022.110970.

Wang, J.B., He, Z.L., Zhu, D.Y., Liu, Q.Y., Ding, Q., Li, S.J., Zhang, D.W., 2020. Petrological and geochemical characteristics of the botryoidal dolomite of Dengying Formation in the Yangtze Craton, South China: Constraints on terminal Ediacaran “dolomite seas”. Sediment. Geol. 406, 105722. https://doi.org/10.1016/j.sedgeo.2020.105722.

Wang, P., Wang, G.W., Chen, Y.Q., Hao, F., Yang, X.Z., Hu, F.J., Zhou, L., Yi, Y., Yang, G., Wang, X.X., Cong, F.Y., 2023. Formation and preservation of ultra-deep high-quality dolomite reservoirs under the coupling of sedimentation and diagenesis in the central Tarim Basin, NW China. Mar. Petrol. Geol. 149, 106084. https://doi.org/10.1016/j.marpetgeo.2022.106084.

Wang, Q.H., Xu, Z.P., Zhang, R.H., Yang, H.J., Yang, X.Z., 2024. New fields, new types of hydrocarbon explorations and their resource potentials in Tarim Basin. Acta Petrol. Sin. 45 (1), 15–32. https://doi.org/10.7623/syxb202401002 (in Chinese).

Wang, Y.Z., Chen, D.Z., Liu, M., Liu, K., Tang, P., 2022. Ediacaran carbon cycling and Shuram excursion recorded in the Tarim Block, northwestern China. Precambr. Res. 377, 106694. https://doi.org/10.1016/j.precamres.2022.106694.

Wei, G.Q., Zhu, Y.J., Zheng, J.F., Yu, G., Ni, X.F., Yan, L., Tian, L., Huang, L.L., 2021. Tectonic lithofacies paleogeography, large-scale source-reservoir distribution and exploration zones of Cambrian subsalt formation, Tarim Basin, NW China. Petrol. Explor. Dev. 48 (6), 1289–1303. https://doi.org/10.1016/S1876-3804(21)60287-2.

Wood, R.A., Zhuravlev, A.Y., Sukhov, S.S., Zhu, M., Zhao, F., 2017. Demise of Ediacaran dolomitic seas marks widespread biomineralization on the Siberian platform. Geology 45 (1), 27–30. https://doi.org/10.1130/G38367.1.

Wu, L., Zhu, G.Y., Yan, L., Feng, X.Q., Zhang, Z.Y., 2021. Late Ediacaran to early Cambrian tectonic–sedimentary controls on lower Cambrian black shales in the Tarim Basin, Northwest China. Global Planet. Change 205, 103612. https://doi.org/10.1016/j.gloplacha.2021.103612.

Xiao, Q., Xia, Z.C., She, Z.B., Papineau, D., Luo, G., Chang, B., Liu, D., Mason, R., Li, M.T., Li, C., 2024. Ubiquitous occurrence of organogenic dolomite in a late Ediacaran limestone-dominated succession from the Eastern Yangtze Gorges area of South China. Precambr. Res. 400, 107269. https://doi.org/10.1016/j.precamres.2023.107269.

Xu, Q.L., Ma, Y.S., Liu, B., Song, X.M., Su, J., Chen, Z.X., 2019. Characteristics and control mechanism of nanoscale pores in lacustrine tight carbonates: Examples from the Jurassic Da'anzhai member in the central Sichuan Basin, China. J. Asian Earth Sci. 178, 156–172. https://doi.org/10.1016/j.jseaes.2018.05.009.

Xu, Z.H., Lan, C.J., Zhang, B.J., Hao, F., Lu, C.J., Tian, X.W., Zou, H.Y., 2022. Impact of diagenesis on the microbial reservoirs of the terminal Ediacaran Dengying Formation from the Central to Northern Sichuan Basin, SW China. Mar. Petrol. Geol. 146, 105924. https://doi.org/10.1016/j.marpetgeo.2022.105924.

Yan, W., Yang, G., Yi, Y., Zuo, X.J., Wang, X.M., Lou, H., Rao, H.W., 2019. Characteristics and genesis of upper Sinian dolomite reservoirs in Keping area, Tarim Basin. Acta Petrol. Sin. 40 (3), 295–307. https://doi.org/10.7623/syxb201903004 (in Chinese).

Yang, H.J., Chen, Y.Q., Wang, B., Yang, W.J., Huang, S.Y., Yang, P.F., Yi, Y., Wang, X.X., 2021. Study on tectonic and sedimentary evolution during the Nanhua-Middle Cambrian and its significance for subsalt exploration, Tarim Basin. China Pet. Explor. 26, 84–98. https://doi.org/10.3969/j.issn.1672-7703.2021.04.007 (in Chinese).

Yang, H.X., Hu, A.P., Zheng, J.F., Liang, F., Luo, X.Y., Feng, Y.X., Shen, A.J., 2020a. Application of mapping and dating techniques in the study of ancient carbonate reservoirs: A case study of Sinian Qigebrak Formation in northwestern

Tarim Basin, NW China. Petrol. Explor. Dev. 47 (5), 1001–1013. https://doi.org/10.1016/S1876-3804(20)60112-4.
Yang, H.X., Shen, A.J., Zheng, J.F., Hu, A.P., 2020b. Sedimentary characteristics and reservoir significance of the microbial dolomite of Sinian Qigebrak Formation in the northwest margin of Tarim Basin. Mar. Orig. Pet. Geol. 25 (1), 44–54. https://doi.org/10.3969/j.issn.1672-9854.2020.01.005 (in Chinese).
Yuan, G.H., Cao, Y.C., Jin, Z.J., Schulz, H.M., Jin, Z.H., Fang, R., Zhao, X.Y., Liu, K.Y., Wang, J.X., 2025. Thermally driven organic-inorganic interactions in sedimentary basins: A review from source rocks to reservoirs. Earth Sci. Rev. 262, 105043. https://doi.org/10.1016/j.earscirev.2025.105043.
Yuan, Y.L., Shi, X.Y., Tang, D.J., Shi, Q., Li, Y., 2022. Microfabrics and organominerals as indicator of microbial dolomite in deep time: An example from the Mesoproterozoic of North China. Precambr. Res. 382, 106881. https://doi.org/10.1016/j.precamres.2022.106881.
Zhai, X.F., Song, J.M., Luo, P., Jin, T.F., Wu, S.T., Wang, S., Wang, G.Q., Li, P.W., 2023. Dolomite porosity related to peritidal microbialites textures and facies succession in Mesoproterozoic Wumishan Formation, North China. Precambr. Res. 389, 107000. https://doi.org/10.1016/j.precamres.2023.107000.
Zhang, P., Huang, K.J., Luo, M., Cai, Y.P., Bao, Z.A., 2022. Constraining the terminal Ediacaran seawater chemistry by Mg isotopes in dolostones from the Yangtze Platform, South China. Precambr. Res. 377, 106700. https://doi.org/10.1016/j.precamres.2022.106700.
Zhang, T., Li, Y.F., Fan, T.L., Lash, G., Gao, Z.Q., Fan, Q., 2020. Marine carbon and sulfur cycling across the Ediacaran-Cambrian boundary in Tarim Block and its implications for paleoenvironmental changes. Paleogeogr. Paleoclimatol. Paleoecol. 560, 110011. https://doi.org/10.1016/j.palaeo.2020.110011.
Zhang, X.F., Cai, Z.X., Li, L., Gu, X.D., Zhao, W.G., 2011. Relict textures of dolomite and the related porosity classification. Acta Sedimentol. Sin. 29 (3), 475–485. https://doi.org/10.14027/j.cnki.cjxb.2011.03.017 (in Chinese).
Zhang, X.F., Liu, B., Wang, J.Q., Zhang, Z., Shi, K.B., Wu, S.L., 2014. Adobe photoshop quantification (PSQ) rather than point-counting: A rapid and precise method for quantifying rock textural data and porosities. Comput. Geosci. 69, 62–71. https://doi.org/10.1016/j.cageo.2014.04.003.
Zhang, Z.Y., Zhu, G.Y., Chen, W.Y., Wu, L., Ren, R., Zhang, C.L., 2024. Cryogenian-Cambrian tectono-sedimentary evolution, paleoclimate and environment effects, and formation of petroleum resources in the Tarim Block. Earth Sci. Rev. 248, 104632. https://doi.org/10.1016/j.earscirev.2023.104632.
Zhao, D.F., Ni, C., Li, S.R., Chen, Y.Q., Qiao, Z.F., Luo, S.C., Wang, Q., Tan, X.C., 2024. Dolomitization history and fluid evolution of end-ediacaran multi-phase dolomites from the near-surface to deep burial depths in the Tarim Craton, northwestern China. Mar. Petrol. Geol. 168, 106929. https://doi.org/10.1016/j.marpetgeo.2024.106929.
Zhao, D.F., Tan, X.C., Hu, G., Wang, L.C., Wang, X.F., Qiao, Z.F., Luo, S.C., Tang, H., 2021. Characteristics and primary mineralogy of fibrous marine dolomite cements in the end-Ediacaran Dengying Formation, South China: Implications for Aragonite-dolomite seas. Paleogeogr. Paleoclimatol. Paleoecol. 581, 110635. https://doi.org/10.1016/j.palaeo.2021.110635.
Zhao, D.F., Zeng, J.J., Tan, X.C., Wang, X.F., Qiao, Z.F., Luo, S.C., 2023a. The coupled evolution of depositional systems and paleo-redox conditions was recorded in terminal Ediacaran sedimentary succession in the Tarim Block, NW China. J. Asian Earth Sci. 249, 105623. https://doi.org/10.1016/j.jseaes.2023.105623.
Zhao, W.Z., Wang, Z.C., Huang, F.X., Zhao, Z.Y., Jiang, H., Xu, Y., 2023b. Hydrocarbon accumulation conditions and exploration position of ultra-deep reservoirs in onshore superimposed basins of China. Acta Petrol. Sinica 44 (12), 2020–2032. https://doi.org/10.7623/syxb201312002 (in Chinese).
Zhao, Y., Wang, C.L., Ning, L., Zhao, H.F., Bi, J., 2022. Pore and fracture development in coal under stress conditions based on nuclear magnetic resonance and fractal theory. Fuel 309, 122112. https://doi.org/10.1016/j.fuel.2021.122112.
Zheng, J.F., Liu, Y., Zhu, Y.J., Liang, F., 2021b. Geochemical features and its geological significances of the upper Sinian Qigeblak Formation in Wushi area, Tarim Basin. J. Palaeogeogr. 23 (5), 983–998. https://doi.org/10.7605/gdlxb.2021.05.063 (in Chinese).
Zheng, J.F., Shen, A.J., Yang, H.G., Zhu, Y.J., Liang, F., 2021a. Geochemistry and geochronology characteristics and their geological significance of microbial dolomite in upper Sinian, NW Tarim Basin. Acta Pet. Sin. 37 (7), 2189–2202. https://doi.org/10.18654/1000-0569/2021.07.13 (in Chinese).
Zhu, D.Y., Liu, Q.Y., He, Z.L., Ding, Q., Wang, J.B., 2020a. Early development and late preservation of porosity linked to presence of hydrocarbons in Precambrian microbialite gas reservoirs within the Sichuan Basin, southern China. Precambr. Res. 342, 105694. https://doi.org/10.1016/j.precamres.2020.105694.
Zhu, D.Y., Liu, Q.Y., Wang, J.B., Hu, G., Ding, Q., 2022. Transition of seawater conditions favorable for development of microbial hydrocarbon source-reservoir assemblage system in the Precambrian. Precambr. Res. 374, 106649. https://doi.org/10.1016/j.precamres.2022.106649.
Zhu, X., Jin, Z.K., Liang, T., Yi, S., Wei, K., Gao, B.S., Shi, L., 2020b. Depositional environment, diagenetic evolution, and their impact on the reservoir quality of the carboniferous KT-II carbonate in the zhanazhol reservoir, Pre-Caspian Basin, Kazakhstan. Mar. Petrol. Geol. 117, 104411. https://doi.org/10.1016/j.marpetgeo.2020.104411.